Chapter 3 Project and Design

The LBNE Project was formed to design and construct the Long-Baseline Neutrino Experiment. The experiment will comprise a new, high-intensity neutrino source generated from a megawatt-class proton accelerator at Fermi National Accelerator Laboratory (Fermilab) directed at a large far detector at the Sanford Underground Research Facility in Lead, SD. A near detector will be located about 500 m downstream of the neutrino production target. LBNE is currently planned as a phased program, with increased scientific capabilities at each phase.

- The experimental facilities are designed to meet the primary scientific objectives of the experiment: (1) fully characterize neutrino oscillations, including measuring the value of the unknown CP-violating phase, δ_{CP}, and determining the ordering of the neutrino mass states, (2) significantly improve proton decay lifetime limits, and (3) measure the neutrino flux from potential core-collapse supernovae in our galaxy.
- The LBNE beamline, based on the existing *Neutrinos at the Main Injector* (NuMI) beamline design, is designed to deliver a wide-band, high-purity ν_μ beam with a peak flux at 2.5 GeV, which optimizes the oscillation physics potential at the 1,300-km baseline. The beamline will operate initially at 1.2 MW and will be upgradable to 2.3 MW utilizing a proton beam with energy tunable from 60 to 120 GeV.
- The full-scope LBNE far detector is a liquid argon time-projection chamber (LArTPC) of fiducial mass 34 kt.

  The TPC design is modular, allowing flexibility in the choice of initial detector size.
- The LBNE far detector will be located 4,850 feet underground, a depth favorable for LBNE's search for proton decay and detection of the neutrino flux from a core-collapse supernova.
- The high-precision near detector and its conventional facilities can be built as an independent project, at the same time as the far detector and beamline, or later.

3.1 LBNE and the U.S. Neutrino Physics Program

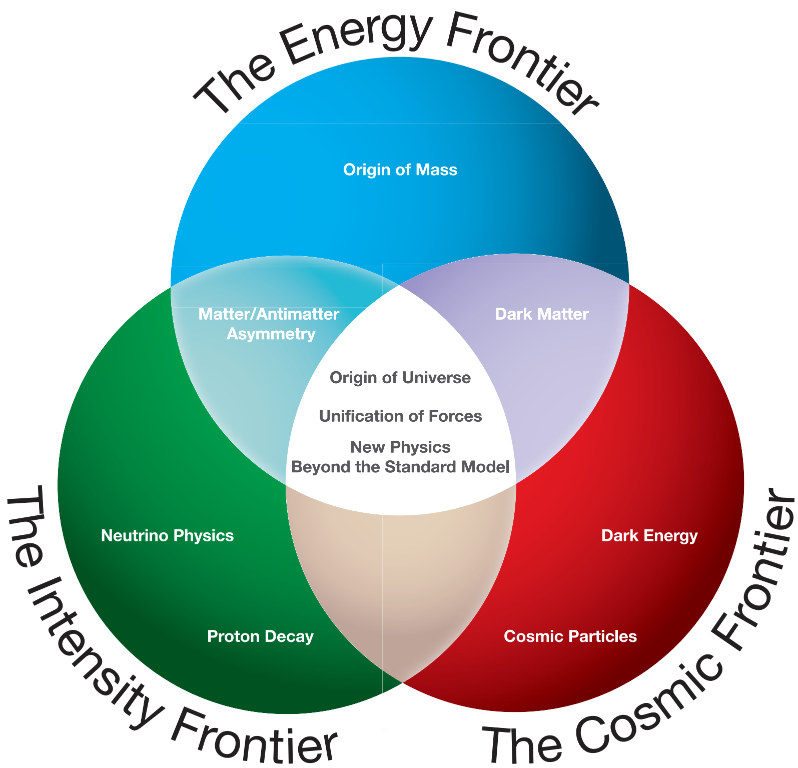

Figure 3.1: Three frontiers of research in particle physics form an interlocking framework that addresses fundamental questions about the laws of Nature and the cosmos. Each frontier, essential to the whole, has a unique approach to making discoveries [1].

In its 2008 report, the U.S. Particle Physics Project Prioritization Panel (P5)* recommended a world-class neutrino physics program as a core component of a U.S. particle physics program [1] that revolves around three research frontiers as shown in Figure 3.1. Included in the report is the long-term vision of a large far detector at the site of the former Homestake Mine in Lead, SD, and a high-intensity, wide-band neutrino source at Fermilab. At the time, the proposed Deep Underground Science and Engineering Laboratory (DUSEL) was planned to occupy the site of the former mine; it is now the Sanford Underground Research Facility.

*P5 is an advisory panel to the two main funding bodies for particle physics in the United States, the Department of Energy (DOE) and the National Science Foundation (NSF).

On January 8, 2010 the DOE approved the Mission Need [2] statement† for a new long-baseline neutrino experiment that would enable this world-class program and firmly establish the U.S. as the leader in neutrino science. The LBNE experiment is designed to meet this Mission Need.

With the facilities provided by the LBNE Project and the unique features of the experiment — in particular the long baseline of 1,300 km, the wide-band beam and the high-resolution, underground far detector — LBNE will conduct a broad scientific program addressing key physics questions concerning the nature of our Universe as described in Chapter 2. The focus of the long-baseline neutrino program will be the explicit demonstration of leptonic CP violation, if it exists, and the determination of the neutrino mass hierarchy.

The 1,300-km baseline has been determined to provide optimal sensitivity to CP violation and the measurement of $\delta_{\rm CP}$, and is long enough to enable an unambiguous determination of the neutrino mass hierarchy [3].

The focus of the non-beam scientific program will be to search for proton decay, to enable detailed studies of atmospheric neutrinos, and to detect and measure the neutrino flux from a supernova, should one occur within our galaxy.

It is currently planned to implement LBNE as a phased program, with increased scientific capabilities at each phase. The initial phase of LBNE will achieve significant advances with respect to its primary scientific objectives as compared to current experiments. The *goal* for the initial phase of LBNE is:

1. A new neutrino beamline at Fermilab driven by a 60 to 120 GeV proton beam with power of up to 1.2 MW.
2. A liquid argon time-projection chamber (LArTPC) detector of fiducial mass at least 10 kt located at the Sanford Underground Research Facility at a depth of 4,850 feet.
3. A high-precision near neutrino detector on the Fermilab site.

The cost for this initial phase (with a 10-kt far detector) is estimated to be 1.2B U.S.$ according to DOE standard project accounting.

In December of 2012, the DOE issued CD-1 (Conceptual Design phase) approval for a budget of 867M$ U.S. based on a reduced scope that excluded the near neutrino detector and the underground placement of the far detector. Domestic and international partners are being sought to enable construction of the full first-phase scope outlined above. Subsequent phases of LBNE are expected to include additional far detector mass and upgrades of the beam to $\geq$2.3-MW capability.

† A *Mission Need* statement initiates the process and provides initial funding toward developing the conceptual design of a DOE scientific project.

3.2 Near Site: Fermi National Accelerator Laboratory

Fermilab, located 40 miles west of Chicago, Illinois, is a DOE-funded laboratory dedicated to high energy physics. The laboratory builds and operates accelerators, detectors and other facilities that physicists from all over the world use to carry out forefront research.

Dramatic discoveries in high energy physics have revolutionized our understanding of the interactions of the particles and forces that determine the nature of matter in the Universe. Two major components of the Standard Model of Fundamental Particles and Forces were discovered at Fermilab: the bottom quark (May-June 1977) and the top quark (February 1995). In July 2000, Fermilab experimenters announced the first direct observation of the tau neutrino, thus filling the final slot in the lepton sector of the Standard Model. Run II of the Fermilab Tevatron Collider was inaugurated in March 2001. The Tevatron was the world's highest-energy particle accelerator and collider until the Large Hadron Collider at CERN came online in 2011.

While CERN now hosts the world's highest-energy particle collider, the Fermilab accelerator complex is being retooled to produce the world's highest-intensity beams of protons, muons and neutrinos. Scientists from around the world can exploit this capability to pursue cutting-edge research in the lepton sector of the Standard Model where strong hints of new physics have surfaced.

The beamline and near detector for LBNE will be constructed at Fermilab, referred to as the *Near Site*.

Fermi National Accelerator Laboratory, originally named the National Accelerator Laboratory, was commissioned by the U.S. Atomic Energy Commission, under a bill signed by President Lyndon B. Johnson on November 21, 1967. On May 11, 1974, the laboratory was renamed in honor of 1938 Nobel Prize winner Enrico Fermi, one of the preeminent physicists of the atomic age.

Today, the DOE operates national laboratories throughout the United States, including Fermilab. The DOE awarded to Fermi Research Alliance (FRA) the management and operating contract for Fermilab, effective January 1, 2007. The FRA is a tax-exempt, limited liability company (LLC) organized and operated for charitable, scientific and educational purposes under Section 501(c)(3) of the Internal Revenue Code. The two members of FRA are the University of Chicago and the Universities Research Association (URA). FRA has earned extensions to the Fermilab contract through Dec. 31, 2015.

At Fermilab, a robust scientific program pushes forward on the three interrelated scientific frontiers specified by the P5 panel in 2008 [1] and illustrated in Figure 3.1:

1. At the Energy Frontier, Fermilab scientists are significant contributors to the LHC and to the CMS experiment.

2. At the Intensity Frontier, Fermilab operates two neutrino beams that support a number of experiments. In the next few years several new neutrino and muon experiments will be coming online, of which LBNE will be the largest.

3. At the Cosmic Frontier, Fermilab runs and/or participates in several experiments, with instruments installed in North America, South America and Europe.

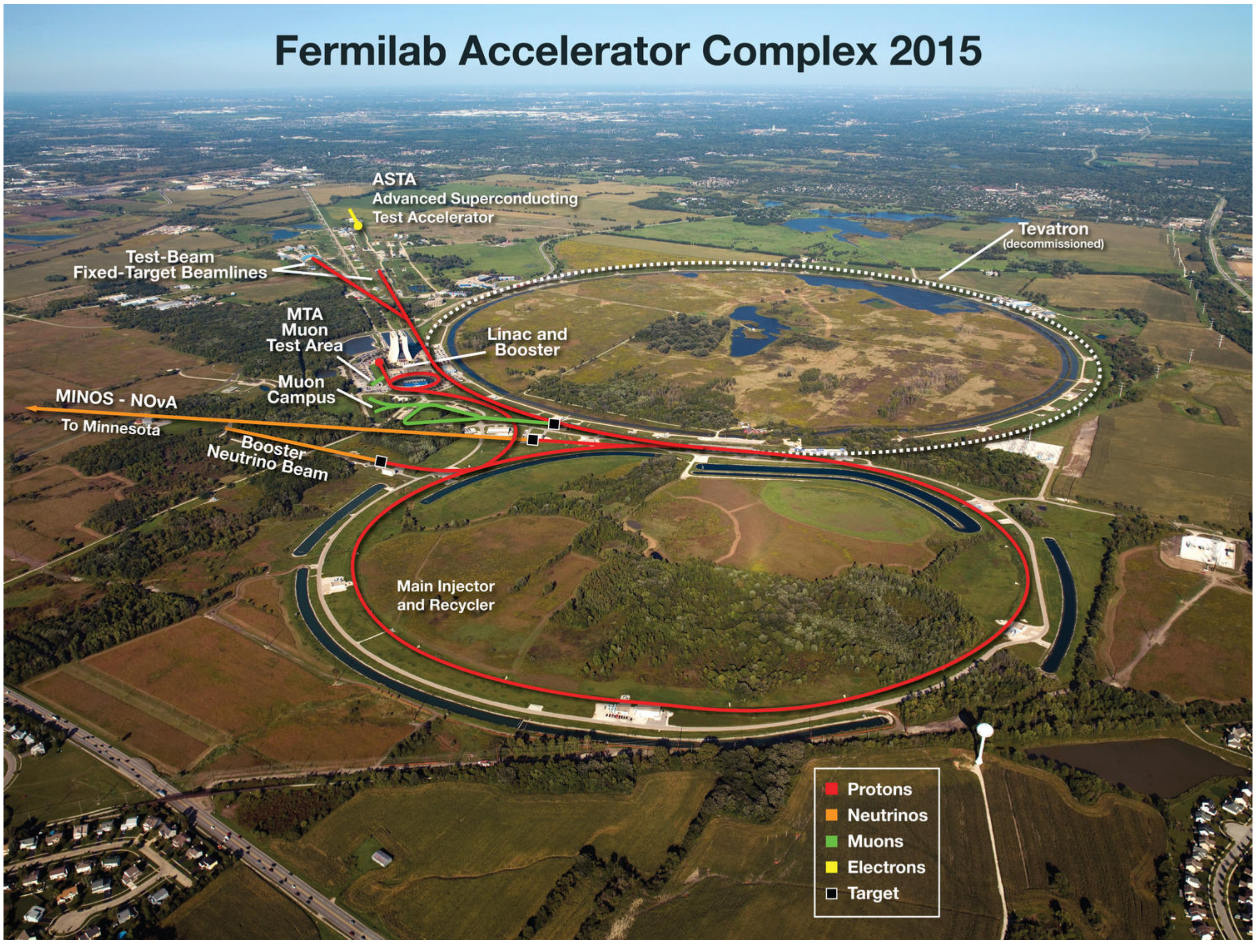

Figure 3.2: The accelerator chain at Fermi National Accelerator Laboratory. A 400-MeV linear accelerator (linac) feeds into the 15-Hz Booster, which produces an 8-GeV beam. The Booster beam is used for the Booster Neutrino Beamline experiments. The Booster feeds into the 120-GeV Main Injector. The Main Injector is the source for the NuMI beamline, which supplies a high-power, high-energy neutrino beam to the MINOS/MINOS+ and NOνA experiments.

The neutrino beams at Fermilab come from two of the lab's proton accelerators (Figure 3.2), the 8-GeV Booster, which feeds the *Booster Neutrino Beamline* (BNB), and the 120-GeV Main Injector (MI), which feeds the NuMI beamline. The LBNE beamline, described in Section 3.4, will utilize the MI beam.

NuMI, on which LBNE's beamline design is based, is a high-energy neutrino beam that has been operating since 2004. It was designed for steady 400-kW operation and achieved that goal by the end of the MINOS experimental run in 2012. As shown in Figure 3.3, the NuMI beamline was running with an average of 9×10^{18} protons per week ($\approx 2.7 \times 10^{20}$ protons-on-target per year) in mid 2012.

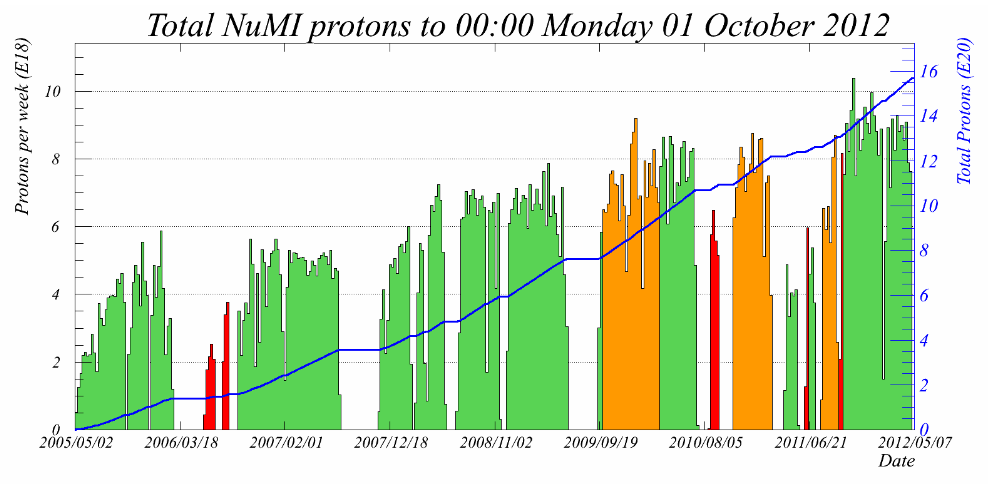

Figure 3.3: The NuMI beamline performance

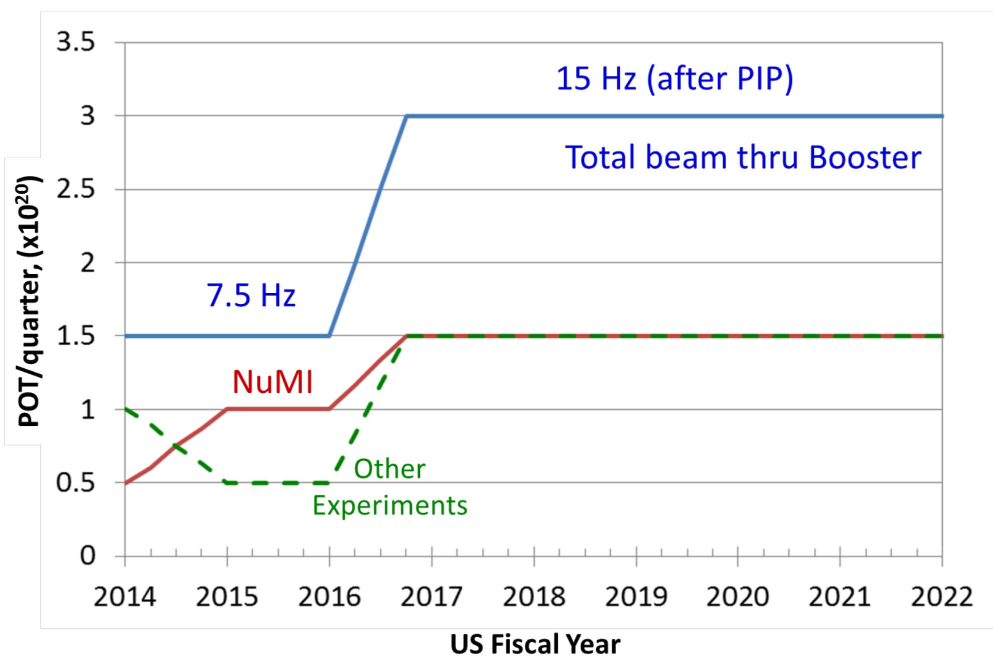

Figure 3.4: A possible ramp-up scenario for proton flux from Fermilab's proton source for the Intensity Frontier experiments.

Upgrades to the Recycler[‡] and MI as part of the NOνA Project, as well as the Proton Improvement Plan (PIP) that is currently underway, comprise a set of improvements to the existing Linac, Booster and MI aimed at supporting 15-Hz beam operations from the Booster (Figure 3.4).

In combination, the NOνA upgrades and the PIP create a capability of delivering 700 kW from the MI at 120 GeV ($\approx 6 \times 10^{20}$ proton-on-target per year) by 2016. The proton beam power expected to be available as a function of MI beam energy after completion of the PIP upgrades is shown in Figure 3.5.

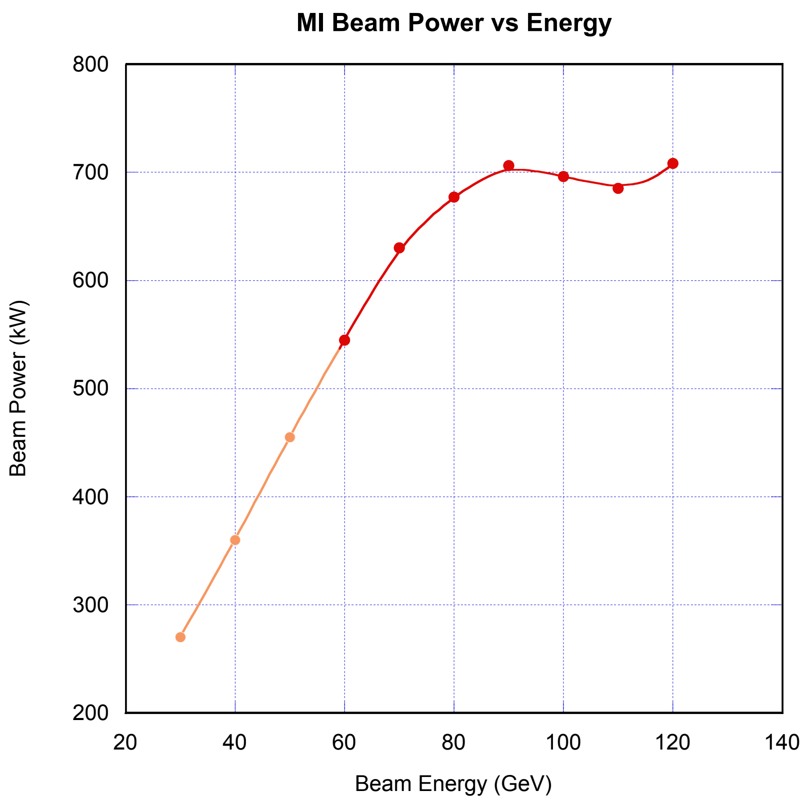

Figure 3.5: Proton beam power expected to be available as a function of MI beam energy after proton-improvement-plan (PIP) upgrades.

A conceptual plan for further upgrades to the Fermilab accelerator complex has been completed. Called the *Proton Improvement Plan-II* (PIP-II) [4], its goal is to increase the capabilities of the existing accelerator complex to support delivery of 1.2 MW of beam power to the LBNE production target at the initiation of operations, while simultaneously providing a platform for subsequent upgrades of the complex to multi-MW capability. The starting point of this plan is the *Project X Reference Design Report* [5].

‡The Recycler, a fixed 8-GeV kinetic energy storage ring located directly above the MI beamline, stores protons from the 8-GeV Booster during MI ramp up.

The primary bottleneck to providing increased beam power at Fermilab is the Fermilab Booster, limited by space-charge forces at injection. In the intermediate term the most cost-effective approach to removing this bottleneck is to increase the injection energy into the Booster. The PIP-II meets this goal via an 800-MeV superconducting linear accelerator (linac), operated at low duty factor, but constructed of accelerating modules that are capable of continuous-wave (CW) operations if provided with sufficient cryogenic cooling and appropriate RF power. This is expected to increase the beam intensity delivered from the Booster by 50% relative to current operations. Shortening the MI cycle time to 1.2 s yields a beam power of 1.2 MW at 120 GeV. The conceptual site layout of PIP-II is shown in Figure 3.6. Further possible upgrades beyond PIP-II would require replacing the 8-GeV Booster with a superconducting linac injecting into the MI at energies between 6 and 8 GeV as shown in Figure 3.6, eventually increasing the power from the MI to 2.0–2.3 MW at 60–120 GeV.

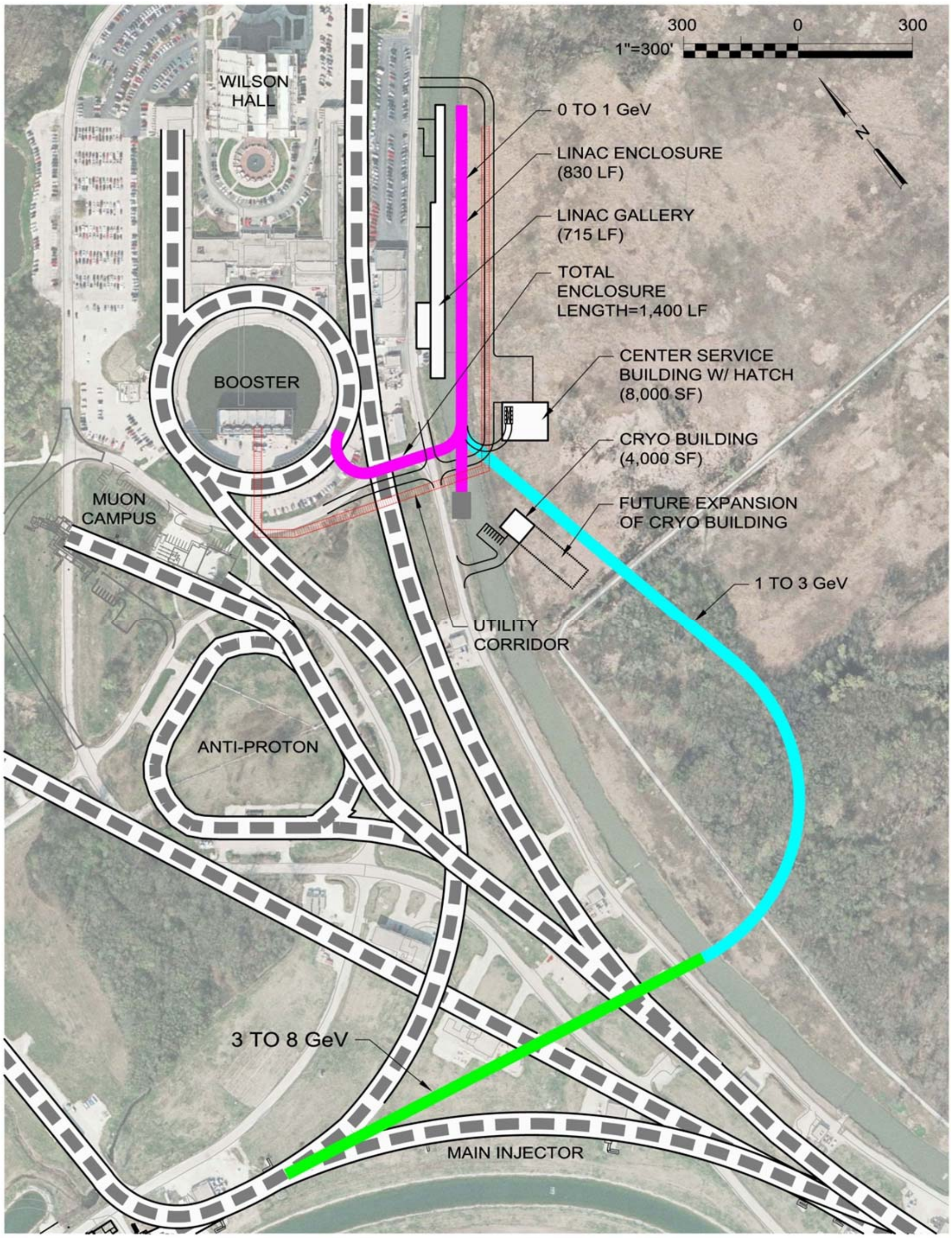

Figure 3.6: Site layout of PIP- II is shown as the magenta line which is the 800 MeV linac enclosure and transfer line. New construction includes the linac enclosure, transfer line enclosure, linac gallery, center service building, utility corridor, and cryo building. Dashed areas represent existing or planned underground enclosures. Further possible upgrades to the Fermilab complex beyond PIP- II are shown in the bottom half of the figure: cyan is a 1-3 GeV CW linac and transfer line, and green is a 3-8 GeV pulsed linac [4].

3.3 Far Site: Sanford Underground Research Facility

The Sanford Underground Research Facility [6] is a laboratory located on the site of the former Homestake gold mine in Lead, SD that is dedicated to underground science. This laboratory has been selected as the location of the far detector for LBNE, and is referred to as the *Far Site*.

Underground neutrino experiments in the former mine date back to 1967 when nuclear chemist Ray Davis installed a solar neutrino experiment 4,850 feet below the surface [7]. Ray Davis earned a share of the Nobel Prize for physics in 2002 for his experiment, which ran until 1993.

LBNE is envisioned as the next-generation, multi-decade neutrino experiment at this site seeking groundbreaking discoveries.

In 2006, Barrick Gold Corporation donated the Homestake Gold Mine site, located in Lead, South Dakota (Figure 3.7) to the State of South Dakota, following over 125 years of mining. Mining operations created over 600 km of tunnels and shafts in the facility, extending from the surface to over 8,000 feet below ground. The mining levels are distributed ∼150 feet apart and are referenced by their depth below the facility entrance, e.g., the level 4,850 feet below ground is referred to as the *4850L*. This former mine encompasses the deepest caverns in the western hemisphere, offering extensive drifts both vertically and laterally. A detailed vertical cross section of the 60 underground levels developed for mining is shown in Figure 3.8.

In 2004, the South Dakota state legislature created the South Dakota Science and Technology Authority (SDSTA) to foster scientific and technological investigations, experimentation and development in South Dakota. A six-member board of directors appointed by the governor of South Dakota directs the SDSTA. The SDSTA's first task was to reopen the former Homestake site to the 4,850-foot level for scientific research. At this site, the SDSTA now operates and maintains the Sanford Underground Research Facility through a contract managed and overseen by a dedicated operations office at Lawrence Berkeley National Laboratory as a deep-underground research laboratory. The Sanford Underground Research Facility property comprises 186 acres on the surface and 7,700 acres underground. The surface campus includes approximately 253,000 gross square feet of existing structures. A surface schematic of the campus is shown in Figure 3.9.

The state legislature has since committed more than $40 million in state funds to the development of the Sanford Underground Research Facility, and the state has also obtained a $10 million Community Development Block Grant to help rehabilitate the site. In addition, a $70 million donation from philanthropist T. Denny Sanford has been used to reopen the site for science and to establish the Sanford Center for Science Education. The initial concepts for the facility were developed with

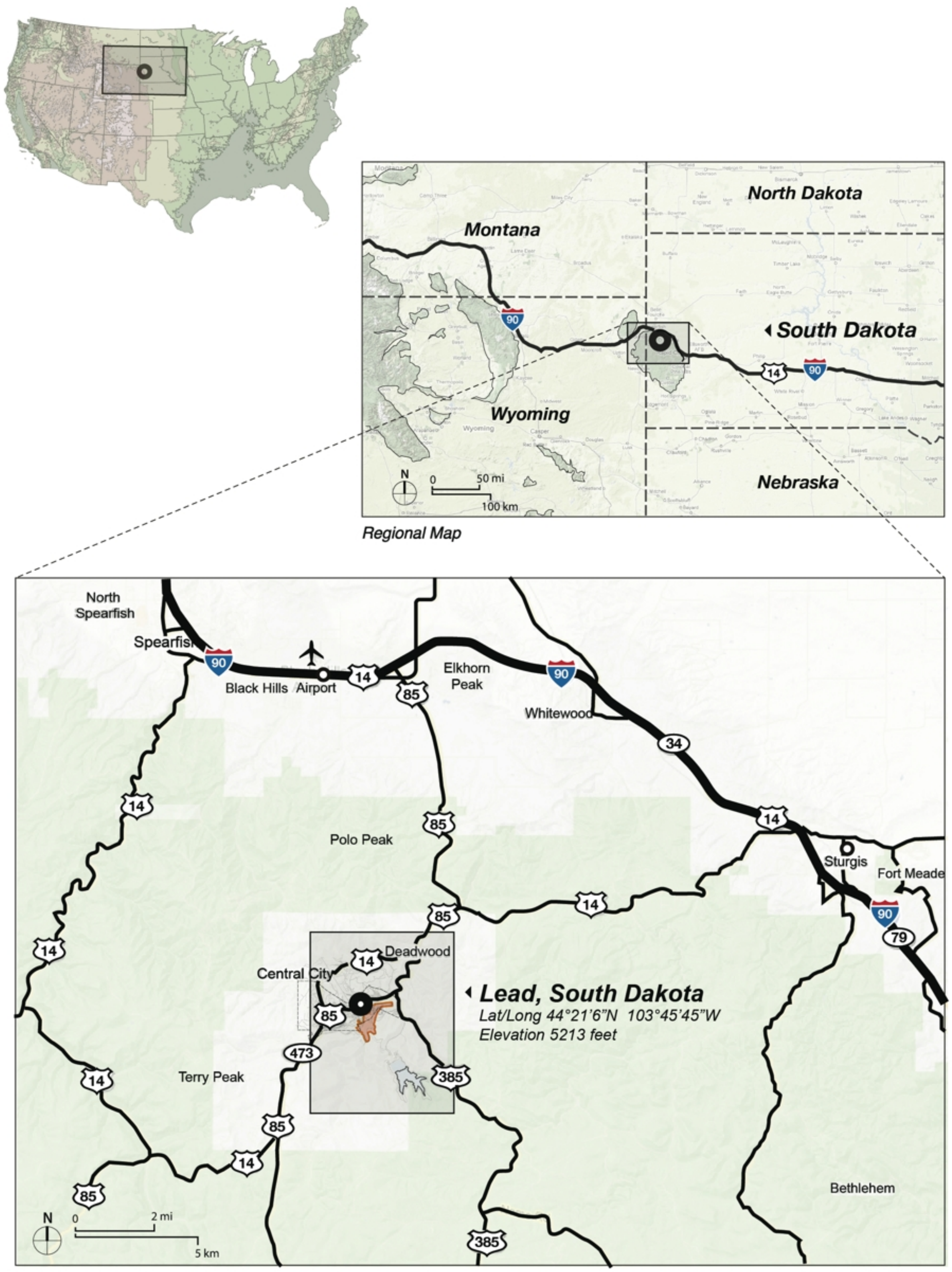

Figure 3.7: Location of the town of Lead, South Dakota - the site of the former Homestake Gold Mine.

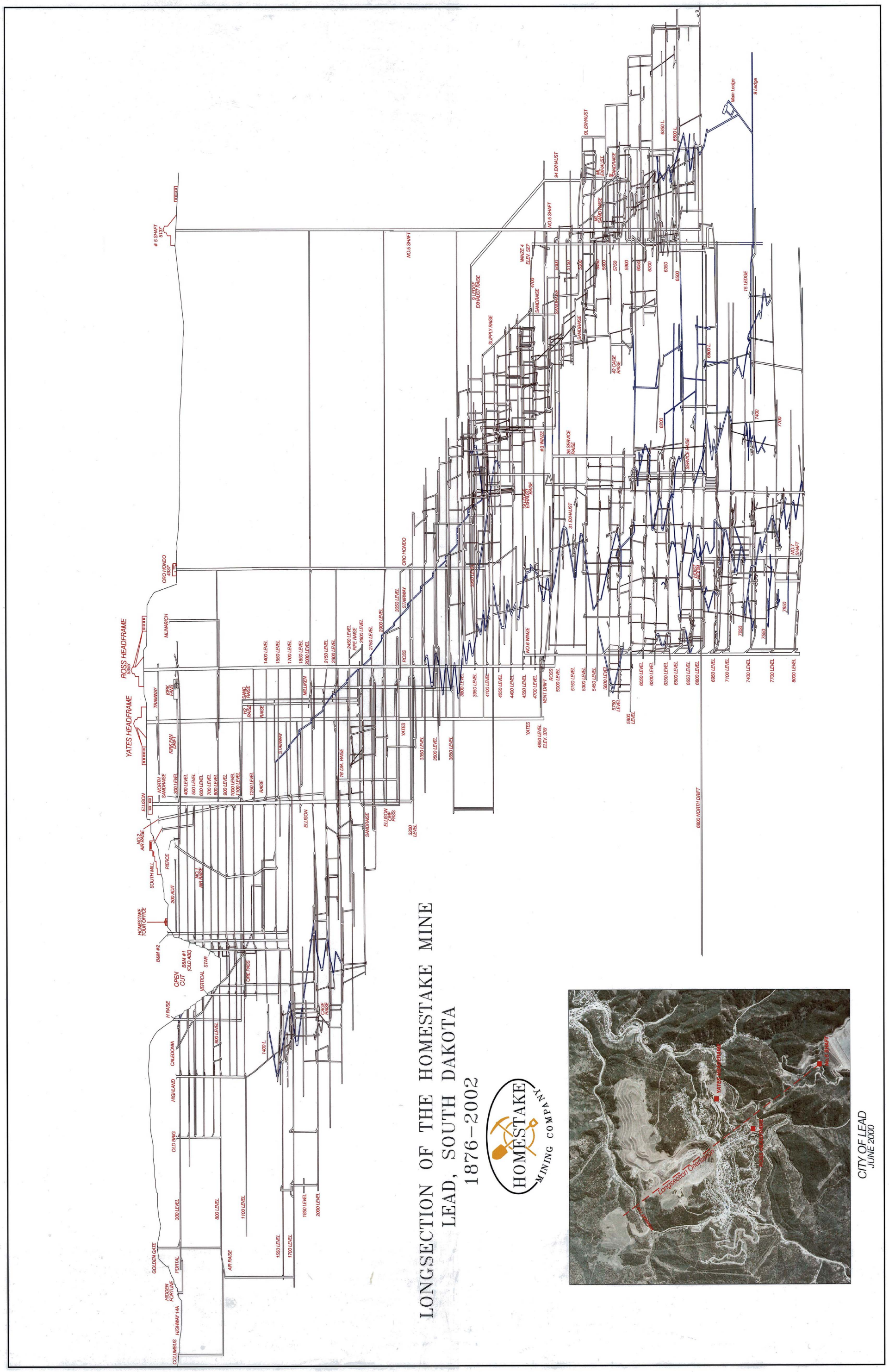

Figure 3.8: The long section of the former Homestake Gold Mine. This figure illustrates the 60 underground levels extending to depths greater than 8,000 feet. The location of cross section is indicated in the inset along a NW to SE plane. The projection extends for 5.2 km along this plane

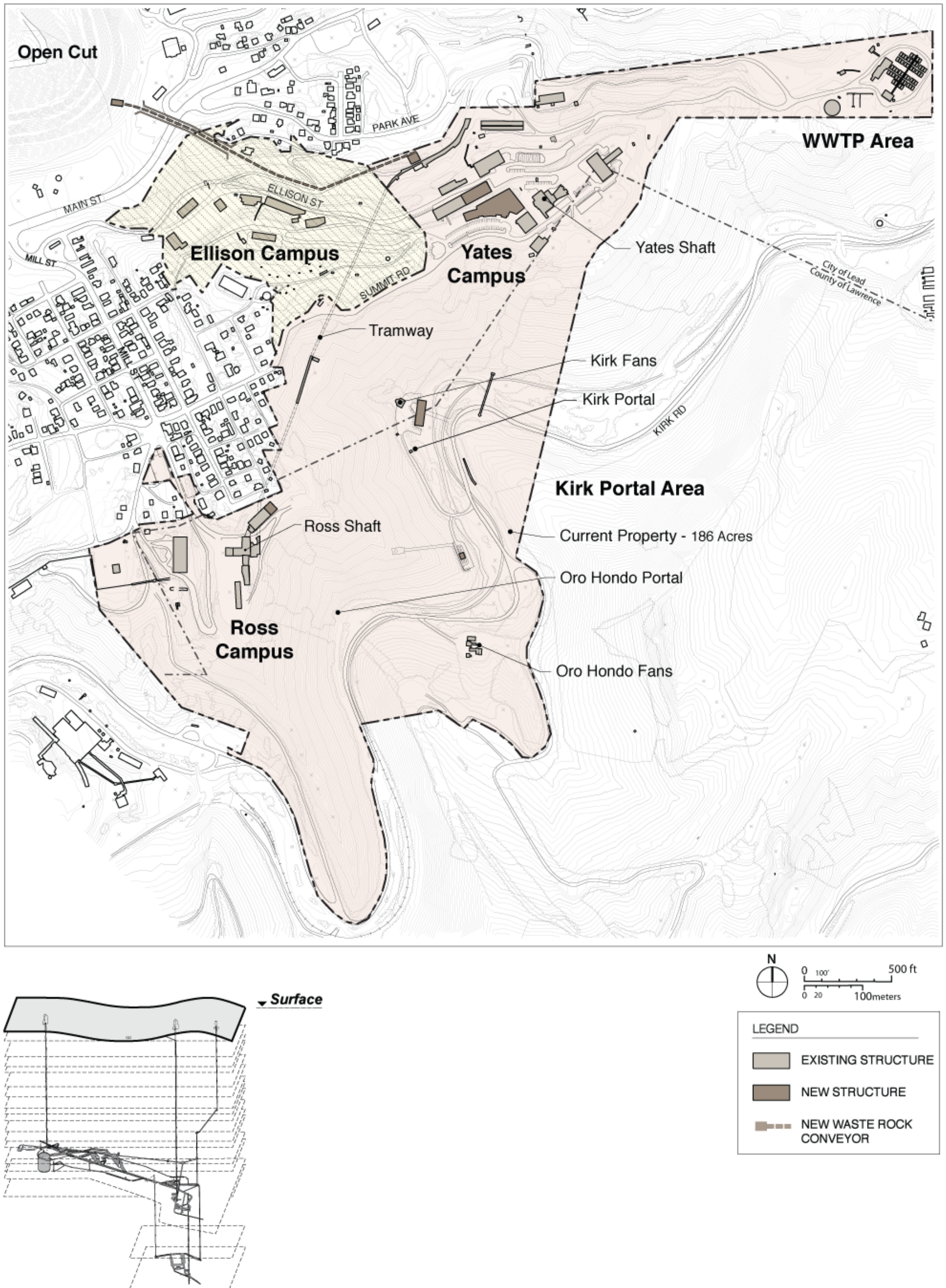

Figure 3.9: The surface and underground campuses of the Sanford Underground Research Facility. The 3D inset image illustrates the plans to develop the 4850L and 7400L. Most current experiments are at the 4850L.

the support of the U.S. National Science Foundation (NSF) as the primary site for the NSF's Deep Underground Science and Engineering Laboratory (DUSEL). With the National Science Board's decision to halt development of the NSF-supported underground laboratory, the DOE now supports the operation of the facility in addition to state and private funding. Both the NSF and the DOE support experiments at the site.

Access to the underground areas has been reestablished and the primary access rehabilitated and improved. The facility has been stabilized and the accumulated underground water has been pumped out below 5,680 ft. The area around the Davis cavern at the 4850L, named for the late Ray Davis, has been enlarged and adapted primarily for current and next-generation dark matter and neutrinoless double-beta decay experiments. This upgraded area of the 4850L is now called the Davis Campus. Additional science efforts are located throughout the facility, including an ultrapure detector development laboratory, geophysics and geological efforts, and a public outreach program. A 3D schematic highlighting the planned development of the 4850L is shown in Figure 3.10. The

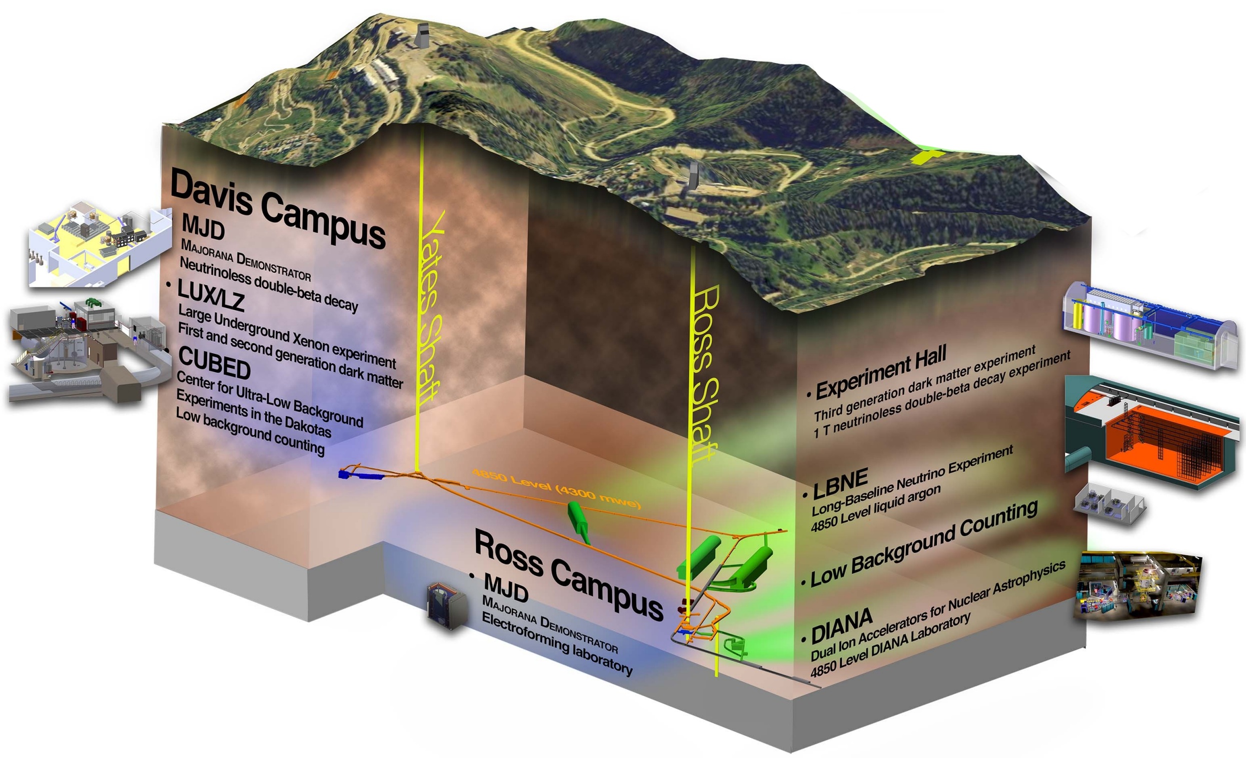

Figure 3.10: Layout of experiments at the 4,850-ft level in the Sanford Underground Research Facility

LBNE far detector will be located in new excavated spaces near the bottom of the Ross Shaft, about 1 km from the Davis Campus. The 4,850-ft depth makes it an extremely competitive location in terms of cosmic-ray background suppression for undertaking the nucleon decay and supernova neutrino studies that LBNE plans to address. Figure 3.11 shows the predicted cosmic-ray flux at this site [8] as compared to other underground laboratories worldwide.

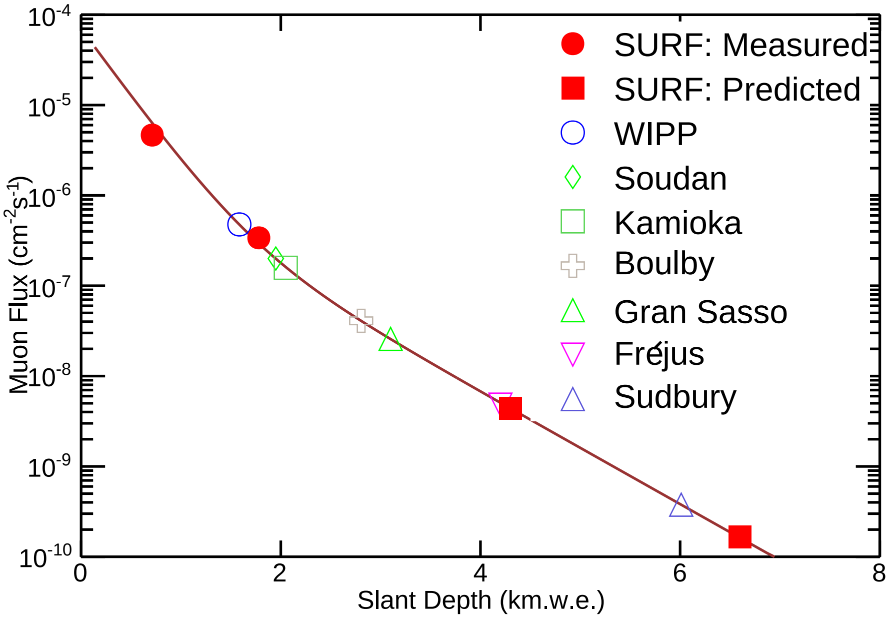

Figure 3.11: Predicted cosmic-ray flux as a function of depth. The predicted muon flux at the 4,850 ft and 8,000 ft levels of the Sanford Underground Research Facility (SURF) are show as red squares. Two measured depths in the facility are shown as red circles. Values for other underground laboratories are also shown [8]. The line shows a parameterized model of the muon flux.

Another advantage of the 4850L Sanford Underground Research Facility site for LBNE is the low level of rock radioactivity that could contribute backgrounds to the supernova burst neutrino signal and other low-energy physics searches. It was found that the U/Th/K radioactivity for the underground bedrocks at Homestake is in general very low when compared to common construction materials such as concrete and shotcrete; some samples are in the sub-ppm levels. However, samples from rhyolite intrusions, *a very small fraction of the total*, show a relatively high content of U, Th, and K more typical of the levels found in other laboratories, in particular those in granitic formations. Regions of potential rhyolite intrusions have been identified and documented as shown in Figure 3.12. In some cases local shielding significantly mitigates the impact of the rhyolite intrusions. Table 3.1 presents some of the assay results, obtained by direct gamma counting for rock samples from the mine, including those collected close to the 4850L [9]. The Large Underground Xenon (LUX) experiment is now operating in the cavern first excavated for Davis in the 1960s. LUX is the most sensitive detector yet to search for dark matter [10]. The Majorana Demonstrator experiment (MJD), also being installed in a newly excavated space adjacent to the original Davis cavern, will search for neutrinoless double-beta decay. Figure 3.13 shows four photographs of facilities and activities at the Sanford Underground Research Facility related to the LUX and MJD at the 4850L. The LBNE far detector will benefit from the common infrastructure being developed to house large experiments underground. The layout of the different proposed experiments at the 4850L, including the LBNE detector, is shown in Figure 3.10.

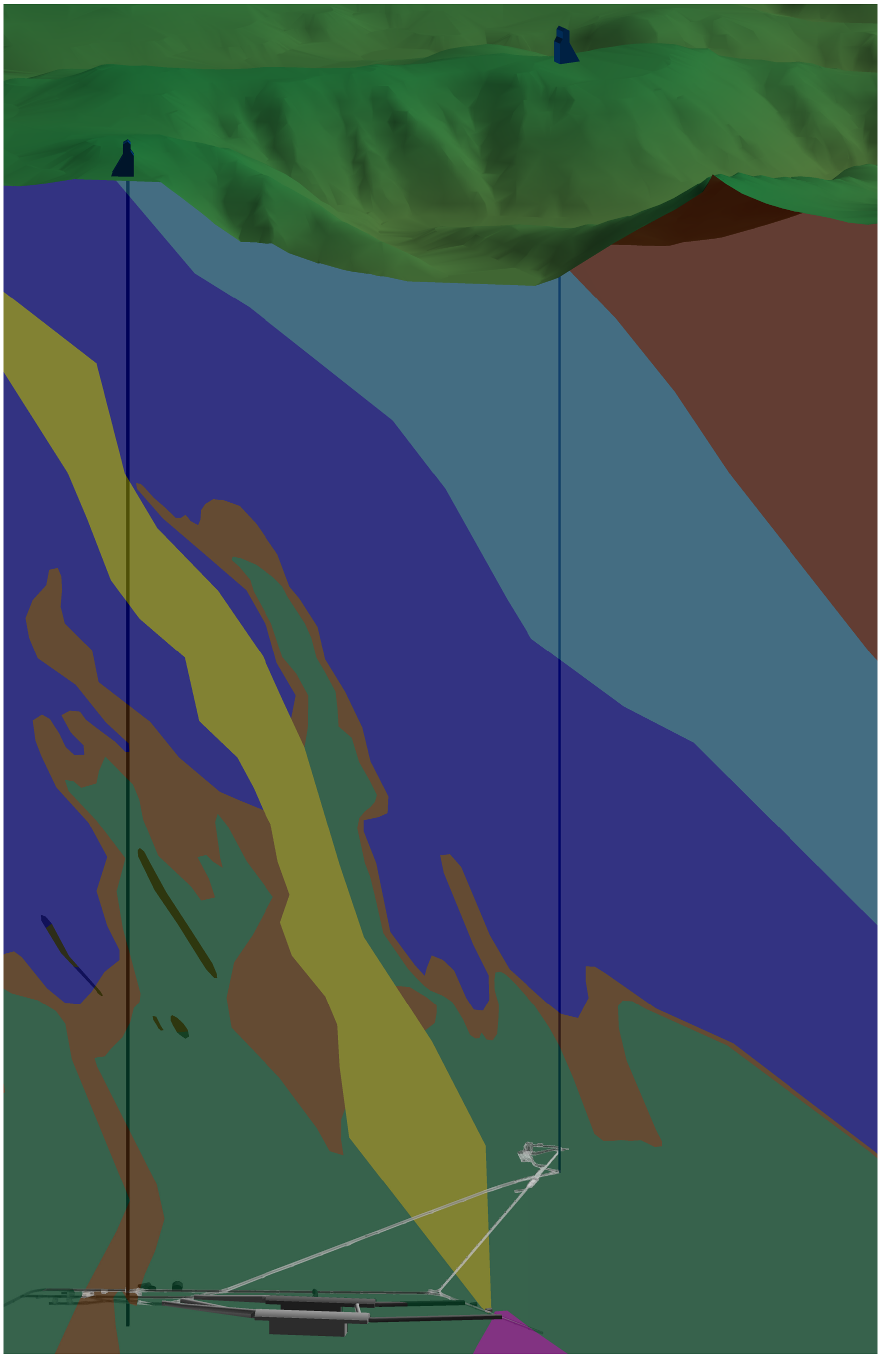

Figure 3.12: Geologic long section of Sanford Underground Research Facility showing the main rock formations. The dark green rock is the Poorman formation, and the yellow areas indicate a projected rhyolite swarm. The proposed location of two LBNE detector caverns are shown in the foreground.

In addition to LBNE, LUX and MJD, the Sanford Underground Research Facility science program for the coming five to ten years (Figure 3.14) consists of the expansion of the LUX dark matter search, the Center for Ultralow Background Experiments at Dakota (CUBED), and the geoscience installations. Long-term plans are being developed to host a nuclear astrophysics program

Table 3.1: Partial U/Th/K assay results for Sanford Underground Research Facility rock samples. Overall errors estimated to be ∼10-20%. Also shown are results for various construction materials (shotcrete/concrete).

	Uranium (ppm) Ave. [Range]	Thorium (ppm) Ave. [Range]	Potassium (%) Ave. [Range]
U/G Country Rock	0.22 [0.06-0.77]	0.33 [0.24-1.59]	0.96 [0.10-1.94]
Shotcrete	1.89 [1.74-2.23]	2.85 [2.00-3.46]	0.88 [0.41-1.27]
Concrete Blocks	2.16 [2.14-2.18]	3.20 [3.08-3.32]	1.23 [1.27-1.19]
Rhyolite Dike	8.75 [8.00-10.90]	10.86 [8.60-12.20]	4.17 [1.69-6.86]

Figure 3.13: Sanford Underground Research Facility: Administration building and Yates shaft headframe (top left); corridor at 4,850 ft (1,480 m) depth leading to clean rooms and experimental halls (top right); billet of radiopure electroformed copper for the MJD experiment being placed on a lathe in a clean room at 4,850 ft depth (bottom left); LUX experiment at 4,850 ft depth (bottom right).

involving underground particle accelerators (CASPAR and DIANA), and second- and third-generation dark matter experiments.

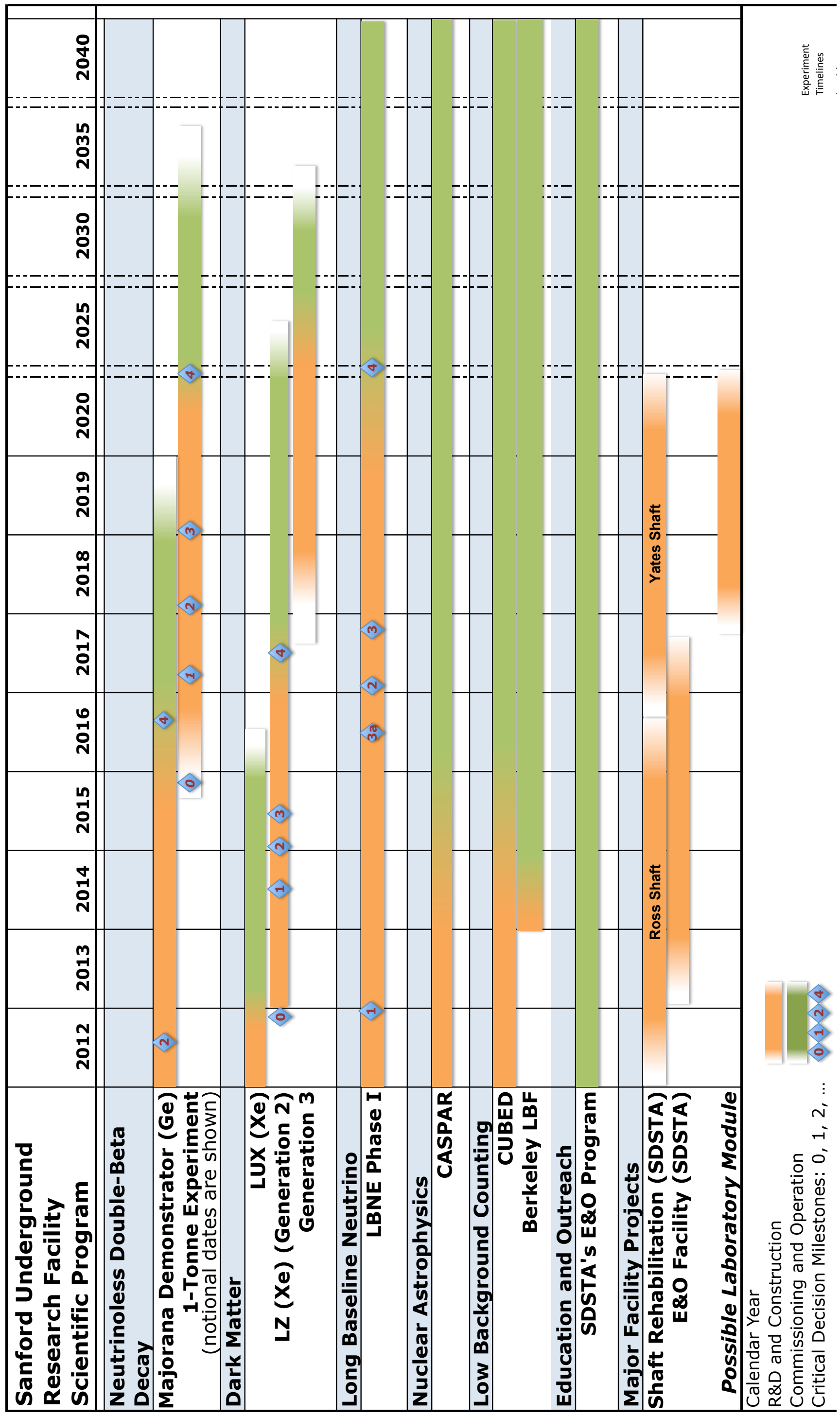

Figure 3.14: Timeline exploring the long-term potential of deep science experiments at the Sanford Underground Research Facility. Figure courtesy of Mike Headley, the Sanford Underground Research Facility.

3.4 Beamline

The LBNE neutrino beamline, located at Fermilab, utilizes a conventional horn-focused neutrino beam produced from pion decay-in-flight, based largely on the highly successful NuMI beamline design:

- The primary beam utilizes 60- to 120-GeV protons from the Main Injector accelerator. The primary beamline is embedded in an engineered earthen embankment — a novel construction concept to reduce costs and improve radiological controls.
- The beamline is designed to operate at 1.2 MW and to support an upgrade to 2.3-MW operation.
- The beamline will generate a wide-band, high-purity beam, selectable for muon neutrinos or muon antineutrinos. Its tunable energies from 60 to 120 GeV will be well matched to the 1,300-km neutrino oscillation baseline.

The LBNE beamline facility will aim a beam of neutrinos toward the LBNE far detector located 1,300 km away at the Sanford Underground Research Facility. The beamline facility, which will be fully contained within Fermilab property, will consist of a primary (proton) beamline, a neutrino beamline, and conventional facilities to support the technical components of the primary and neutrino beamlines [11]. The LBNE beamline reference design parameters approved at CD-1 are summarized in Table 3.2. Improvements to this design that have been made or are being considered are described in this section, including the important change to an initial beam power of 1.2 MW, enabled by the planned PIP-II. The beamline needed for the full-scope LBNE will be realized in the first phase of LBNE and will be upgradable to 2.3 MW.

The primary beam, composed of protons in the energy range of 60-120 GeV, will be extracted from the MI-10 straight section of the Main Injector using single-turn extraction. The beam will then be transported to the target area within a beam enclosure embedded in an engineered earthen embankment (hill). The primary-beam transport section is designed for very low losses. The embankment's dimensions are designed to be commensurate with the bending strength of the required dipole magnets so as to provide a net 5.8° downward vertical bend to the neutrino beam (Figures 3.15 and 3.16). The beamline is then buried by soil shielding that is placed at a stable angle of repose, resulting in the embankment final geometry.

For 120-GeV operation and with the MI upgrades implemented for the NOνA experiment [14], the fast, single-turn extraction will deliver 4.9×10^{13} protons to the LBNE target in a 10-µs pulse. With a 1.33-s cycle time, the beam power for NOνA is 700 kW. Additional accelerator upgrades planned as PIP-II [4] will increase the protons per cycle to 7.5×10^{13} and reduce the cycle time to 1.2 s,

Table 3.2: Partial set of parameters for the elements of the LBNE Beamline reference design at CD-1 from Volume 2 of the CDR [11]. The reference design described a 700 kW beam; it has since been changed to 1.2 MW. For each parameter the third column lists the range that had been studied prior to CD-1. Distances between beam elements are given from the upstream face (the end facing the proton beam) with respect to the upstream (front) face of Horn 1.

Element	Parameter	Range studied	Reference design value (700 kW)
Proton Beam	energy	60 GeV to 120 GeV	120 GeV
	protons per pulse		4.9×10^{13}
	cycle time between pulses		1.33 s
	size at target $\sigma_{x,y}$	1 mm to 2 mm	1.3 mm
	duration		1.0×10^{-5} sec
	POT per year		6.5×10^{20}
Target	material	graphite, beryllium hybrid [12]	graphite
	length	$\geq$ 2 interaction lengths	966 mm
	profile	rectangular, round ($r = 5$ mm to 16 mm)	rectangular 7.4 mm x 15.4 mm
	dist. from Horn 1 (front)	0 cm to −250 cm	−35 cm to −285 cm
Focusing Horn 1 [13]	shape	cylindrical-parabolic, double-parabolic	double-parabolic (NuMI)
	length (focusing region)	2,500 mm to 3,500 mm	3,000 mm
	current	180 kA to 350 kA	200 kA
	minimum inner radius		9.0 mm
	maximum outer radius		174.6 mm
Focusing Horn 2	shape	double-parabolic	NuMI Horn 2
	length (focusing region)	3,000 mm to 4,000 mm	3,000 mm
	current	180 kA to 350 kA	200 kA
	minimum inner radius		39.0 mm
	maximum outer radius		395.4 mm
	dist. from Horn 1 (front)	4,000 mm to 10,000 mm	6,600 mm
Decay Pipe	length	200 m to 350 m	204 m
	radius	1.0 m to 3.0 m	2 m
	atmosphere	Air, He, vacuum	air at atm. pressure
	dist. from Horn 1 (front)	11 m to 23 m	17.3 m

resulting in an initial beam power for LBNE of 1.2 MW. The LBNE beamline is designed to support additional beam power upgrades beyond PIP-II, discussed in Section 3.2, that can increase the beam power up to 2.3 MW. At 1.2-MW operation the accelerator and primary beamline complex are expected to deliver 11×10^{20} protons per year to the target.

Approximately 85% of the protons interact with the solid target, producing pions and kaons that subsequently get focused by a set of magnetic horns into a decay pipe where they decay into muons and neutrinos (Figure 3.17). The neutrinos form a wide-band, sign-selected neutrino or antineutrino

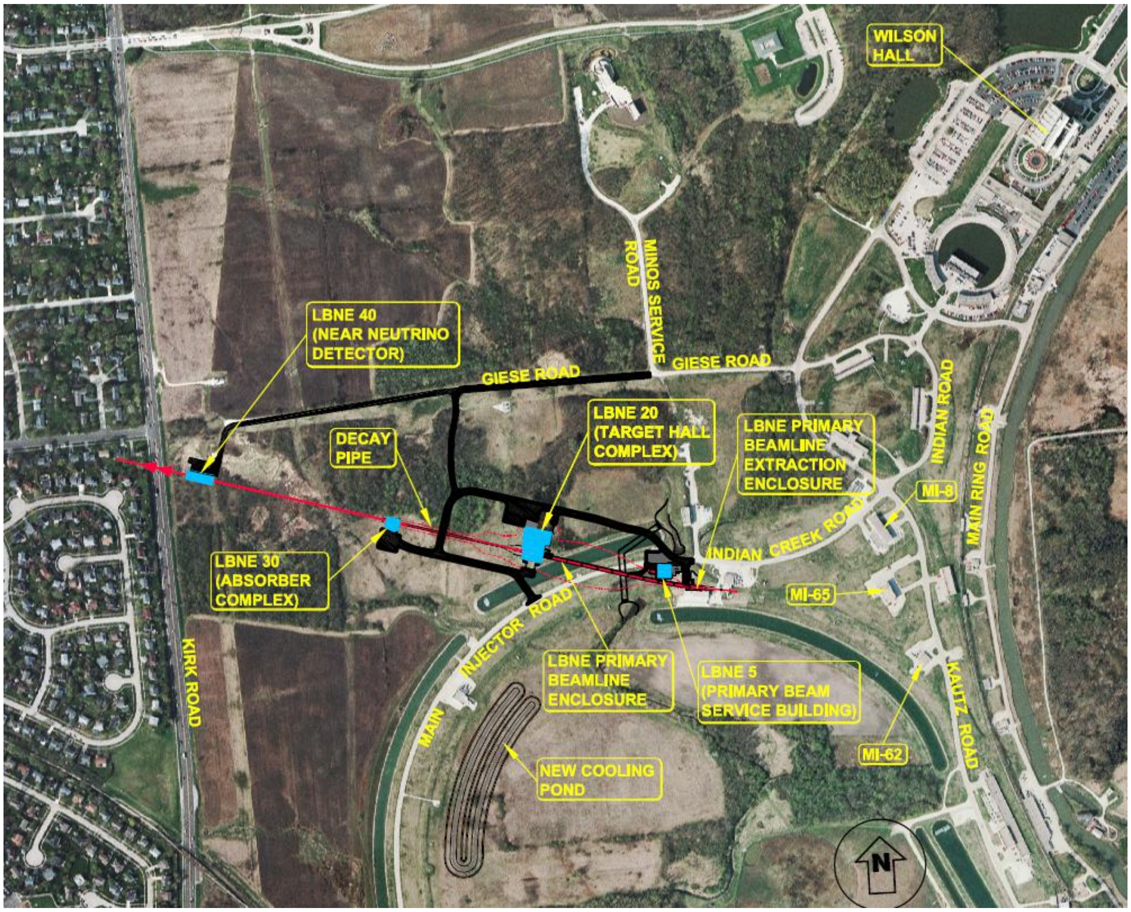

Figure 3.15: Plan view of the overall Near Site project layout showing locations for the LBNE Beamline extraction point from the MI, the primary beamline, target hall, decay pipe, absorber and near neutrino detector.

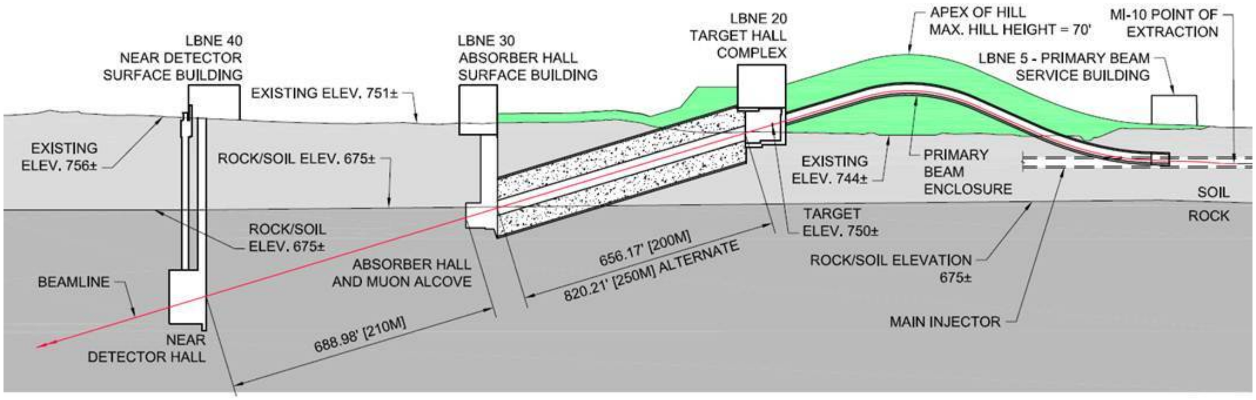

Figure 3.16: Longitudinal section of the LBNE Beamline facility. The beam enters from the right in the figure, the protons being extracted from the MI-10 extraction point at the Main Injector.

beam, designed to provide flux in the energy range of 0.5 to 5 GeV. This energy range will cover the first and second neutrino-oscillation maxima, which for a 1,300-km baseline are at approximately 2.5 and 0.8 GeV, respectively.

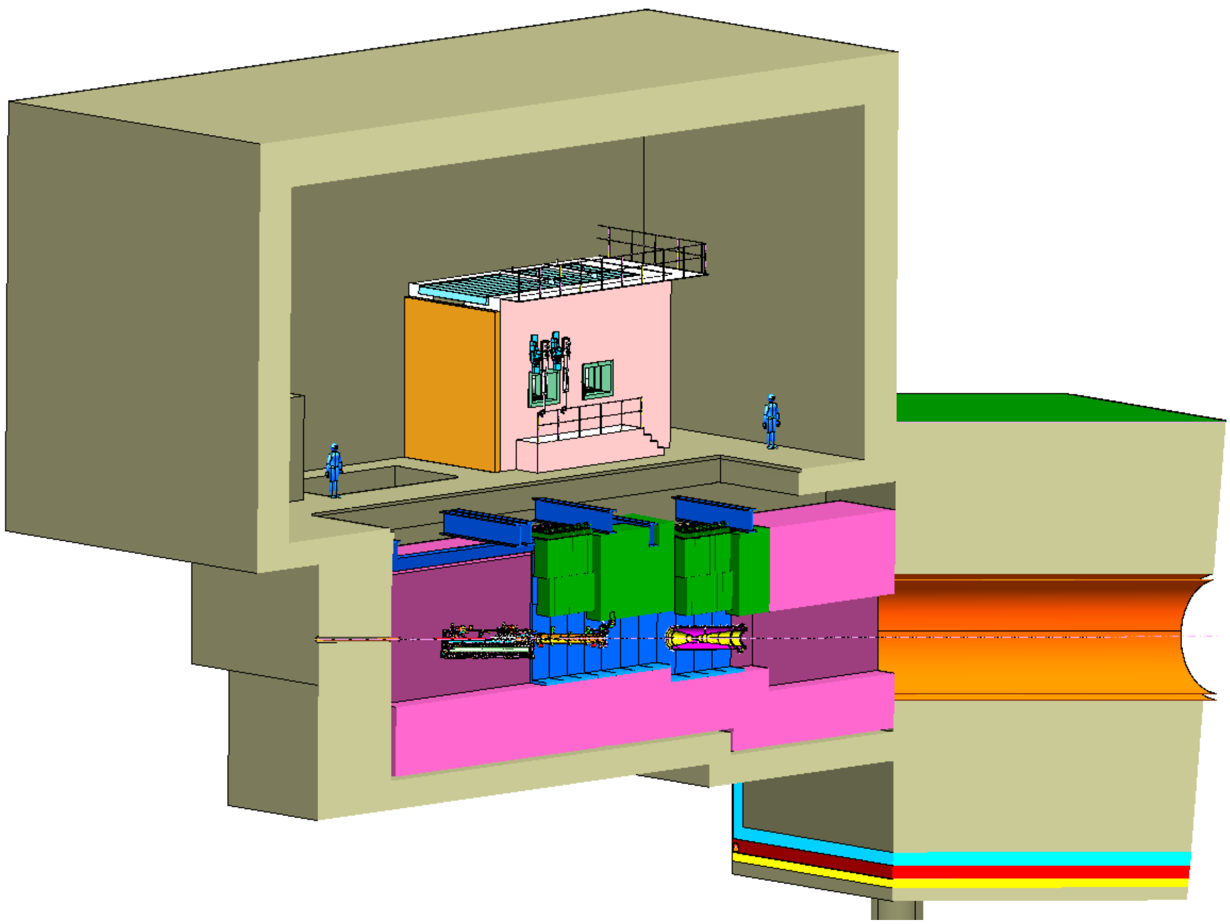

Figure 3.17: Schematic of the upstream portion of the LBNE neutrino beamline showing the major components of the neutrino beam. The target chase bulk steel shielding is shown in magenta. Inside the target chase from left to right (the direction of the beam) pointing downwards: the beam window, horn-protection baffle and target mounted on a carrier, the two toroidal focusing horns (the green custom shielding blocks are part of the horn support modules that are not shown) and the decay pipe (orange). Above the chase and to the right is the work cell for horn and target system repairs. The beige areas indicate concrete shielding.

The reference target design for LBNE is an upgraded version of the NuMI-LE (Low Energy) target that was used for eight years to deliver beam to the MINOS experiment. The target consists of 47 segments, each 2 cm long, of POCO graphite ZXF-5Q. Focusing of charged particles is achieved by two magnetic horns in series, the first of which partially surrounds the target. They are both NuMI/NOνA-design horns with double-paraboloid inner conductor profiles. The NuMI/NOνA-design horns currently operate at 185 kA to 200 kA. The horns have been evaluated and found to be operable with currents up to 230 kA but the striplines that supply the horn currents are still under evaluation. Additional development of the target and horns is required to adapt the existing designs from the 700-kW beam power used by NOνA to 1.2 MW for LBNE. The horn current polarity can be changed to selectively focus positive or negative hadrons, thus producing high purity ($> 90\%$ in oscillation region) ν_μ or $\overline{\nu}_\mu$ beams. Each beam polarity will have a $< 10\%$ contamination of neutrinos of the "wrong sign" in the oscillation energy region ($\overline{\nu}$'s in the ν beam and vice-versa) from decays of wrong-sign hadrons that propagate down the center of the focusing horns — where there is no magnetic field — into the decay volume. In addition, a $\leq 1\%$ contamination of ν_e and $\overline{\nu}_e$ in the ν_e appearance signal region is produced by the decays of tertiary muons from pion decays, and decays of kaons. The neutrino flux components from the LBNE CD-1 beamline design produced using a full Geant4 simulation of both horn polarities are shown in Figure 3.18. The

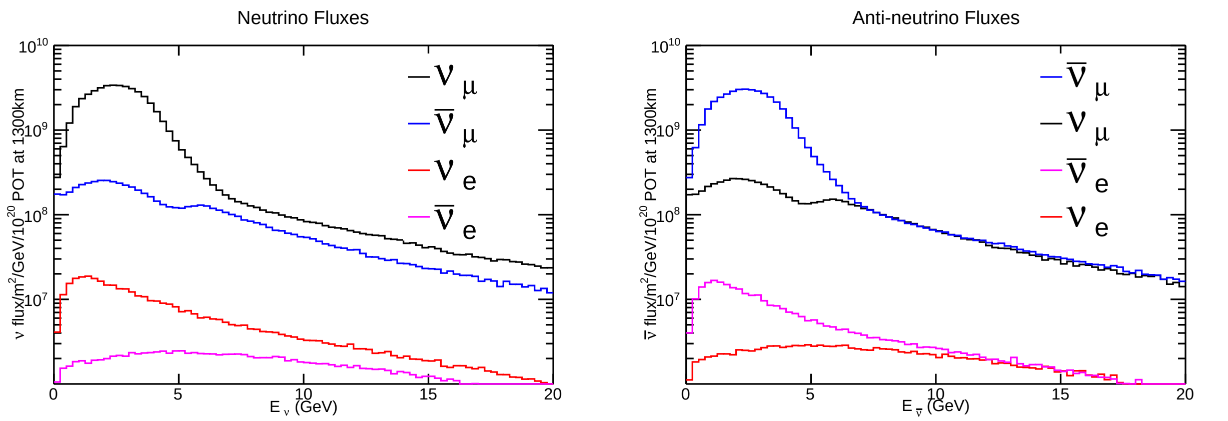

Figure 3.18: The neutrino beam fluxes (left) and antineutrino beam fluxes (right) produced by a Geant4 simulation of the LBNE beamline. The horn current assumed is 200 kA, the target is located 35 cm in front of horn 1, the decay pipe is air-filled, 4 m in diameter and 204 m in length.

beamline design provides a wide-band neutrino beam with a peak flux at 2.5 GeV, which matches the location of the first $\nu_\mu \to \nu_e$ oscillation maximum. The NuMI reference target design used for LBNE allows the target to be moved with respect to Horn 1. The location of the upstream face [§] of the target with respect to the upstream face of Horn 1 can be varied from -35 cm (default location) to -2.85 m, thus the LBNE beamline can produce a wide range of beam spectra. Three possible far-site beam spectra, produced by moving the target from -35 cm (low-energy) to -1.5 m (medium-energy) to -2.5 m (high energy) are shown in Figure 3.19.

The decay volume design for LBNE is a helium-filled, air-cooled pipe of circular cross section with a diameter of 4 m and length from 204 m to 250 m optimized such that decays of the pions and kaons result in neutrinos in the energy range useful for the experiment. A 250-m decay pipe is the maximum length that will allow the near neutrino detector complex to fit within the Fermilab site boundaries. At the end of the decay region, the absorber, a water-cooled structure of aluminum and steel, is designed to remove any residual hadronic particles; it must absorb a large fraction of the incident beam power of up to 2.3 MW. Instrumentation immediately upstream of the absorber

[§] The proton beam direction determines the upstream and downstream conventions. The upstream (front) face of Horn 1 is therefore the Horn 1 face closest to the proton beam window.

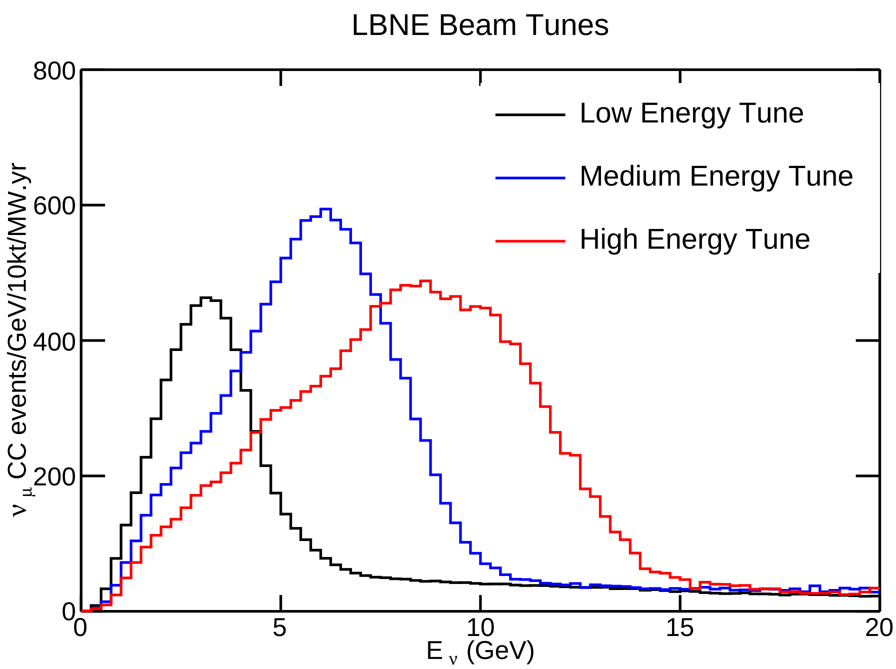

Figure 3.19: Event interaction rates at the LBNE far detector in the absence of oscillations and due to neutrinos produced by a 120 GeV proton beam for several target positions relative to Horn 1. The black curve shows the expected interaction spectrum for the low-energy tune (LE) where the upstream face of the target is located 35 cm upstream of Horn 1, the blue curve is a sample medium-energy (ME) tune with the target located 1.5 m upstream of Horn 1 and the red curve is the high-energy tune (HE) with the target located 2.5 m upstream of Horn 1. The horn current assumed is 200 kA, the decay pipe is air-filled, 4 m in diameter and 204 m in length.

measures the transverse distribution of the resultant hadronic showers to monitor the beam on a pulse-by-pulse basis.

An array of muon detectors in a small alcove immediately downstream of the absorber measures tertiary-beam muons and thereby indirectly provides information on the direction, profile and flux of the neutrino beam. This will be described in Section 3.5.

The beamline conventional facilities include the civil construction required to house the beamline components in their planned layout as shown in Figures 3.15 and 3.16. Following the beam from southeast to northwest, or roughly from right to left in Figure 3.15, the elements include the underground Extraction Enclosure, the Primary Beam Enclosure (inside the embankment) and its accompanying surface-based Service Building (LBNE 5), the Target Complex (LBNE 20) located in the embankment, the Decay Pipe, the underground Absorber Hall with the muon alcove, and its surface-based Service Building (LBNE 30). The embankment will need to be approximately 290 m long and 18 m above grade at its peak. The planned near neutrino detector facility is located as near as is feasible to the west site boundary of Fermilab, along the line-of-sight indicated in red in Figure 3.15.

The parameters of the beamline facility were determined taking into account several factors including the physics goals, the Monte Carlo modeling of the facility, spatial and radiological constraints and the experience gained by operating the NuMI facility at Fermilab. The relevant radiological concerns, prompt dose, residual dose, air activation and tritium production have been extensively modeled and the results implemented in the system design. The beamline facility design described above minimizes expensive underground construction and significantly enhances capability for ground-water radiological protection. In general, components of the LBNE beamline system that cannot be replaced or easily modified after substantial irradiation are being designed for 2.3-MW operation. Examples of such components are the shielding of the target chase and decay pipe, and the absorber with its associated shielding.

The following LBNE beamline design improvements beyond the CD-1 conceptual design are being assessed:

- An increase in the length of the decay pipe up to 250 m (the maximum length allowed by the existing Fermilab site boundaries), and also possibly an increase in its diameter up to 6 m. Increases to the decay pipe size would require additional cost of the order several tens of millions of dollars. Increasing the length of the decay pipe from 200 to 250 m increases the overall event rate in the oscillation region by 12%. Increases in the decay pipe diameter produce a 6% increase in the low-energy neutrino event rate as shown in Table 3.3.
- It has recently been decided to fill the decay pipe with helium instead of air. The total ν_μ event rate increases by about 11%, with a decrease in $\overline{\nu}$ contamination in the neutrino beam. Introducing helium in the decay pipe requires the design and construction of a decay pipe window.
- An increase in the horn current of the horns by a modest amount (from 200 kA to 230 kA); this is expected to increase the neutrino event rates by about 10-12% at the first oscillation maximum [15]. A Finite Element Analysis simulation and a cooling test of the horns are underway to evaluate this option.
- Use of an alternate material to the POCO graphite for the target to increase the target longevity. This would involve additional R&D effort and design work. A beryllium target, for example, could be made shorter, potentially improving the horn focusing.
- Development of more advanced horn designs that could boost the low-energy flux in the region of the second oscillation maximum. It should be noted that the target and horn systems can be modified or replaced even after operations have begun if improved designs enable higher beam flux.

Table 3.3 summarizes the impact of the beam design improvements after CD-1 and the additional costs required. Together, the changes are anticipated to result in an increase of $\sim 50\%$ in the ν_e

appearance signal rate at the far detector. A 30% increase in signal event rate at the far detector can be achieved for < 10 M$ without changing the CD-1 decay pipe size (4 m diameter $\times$ 204 m length) by changing from an air-filled to a helium-filled decay pipe. Increasing the decay pipe size to 6 m diameter $\times$ 250 m length would result in an additional 15% increase in flux but would cost an additional ~ 47 M$ — this includes the cost of a redesigned absorber.

Table 3.3: Impact of the beam improvements under study on the neutrino $\nu_\mu \to \nu_e$ CC appearance rates at the far detector in the range of the first and second oscillation maxima, shown as the ratio of appearance rates: the *improved* rate divided by the rate from the beam design described in the Conceptual Design Report.

Changes	0.5 to 2 GeV	2 to 5 GeV	Extra Cost
Horn current 200 kA $\to$ 230 kA	1.00	1.12	none
Proton beam 120 $\to$ 80 GeV at constant power	1.14	1.05	none
Target NuMI-style graphite $\to$ Be cylinder	1.10	1.00	$<$ 1 M$
Decay pipe Air $\to$ He	1.07	1.11	$\sim$ 8 M$
Decay pipe diameter 4 m $\to$ 6 m	1.06	1.02	$\sim$ 17 M$
Decay pipe length 200 m $\to$ 250 m	1.04	1.12	$\sim$ 30 M$
Total	**1.48**	**1.50**	

3.5 Near Detector

A high-resolution near neutrino detector located approximately 500 m downstream of the LBNE neutrino production target, as shown in Figure 3.16, is a key component of the full LBNE scientific program:

- The near neutrino detector will enable the LBNE experiment to achieve its primary scientific goals — in particular discovery-level sensitivity to CP violation and high-precision measurements of the neutrino oscillation parameters, including the unknown CP-violating phase, $\delta_{\rm CP}$.
- A rich program of LBNE physics measurements at the near detector will exploit the potential of high-intensity neutrino beams as probes of new physics.

To achieve the precision required to make a significant advancement in the measurement of neutrino oscillation parameters over current experiments and to reach the desired 5σ sensitivity to CP violation (discussed in Chapters 4 and 7), LBNE will need to measure the unoscillated flux spectrum, to a few percent, for all neutrino species in the beam: ν_μ, ν_e, $\overline{\nu}_\mu$ and $\overline{\nu}_e$. This requires a high-resolution, magnetized near neutrino detector with high efficiency for identifying and measuring electrons and muons. To measure the small ν_e contamination in the beam with greater precision, the detector would need to be able to distinguish e^+ from e^-; this would require a low-density detector with a commensurately long physical radiation length. In addition, use of an argon target nucleus — similar to the far detector — would allow cancellation of systematic errors. A reference design has been developed for a near neutrino detector that will meet these requirements; in particular it will measure the neutrino event rates and cross sections on argon, water and other nuclear targets for both ν_e and ν_μ charged current (CC) and neutral current (NC) scattering events.

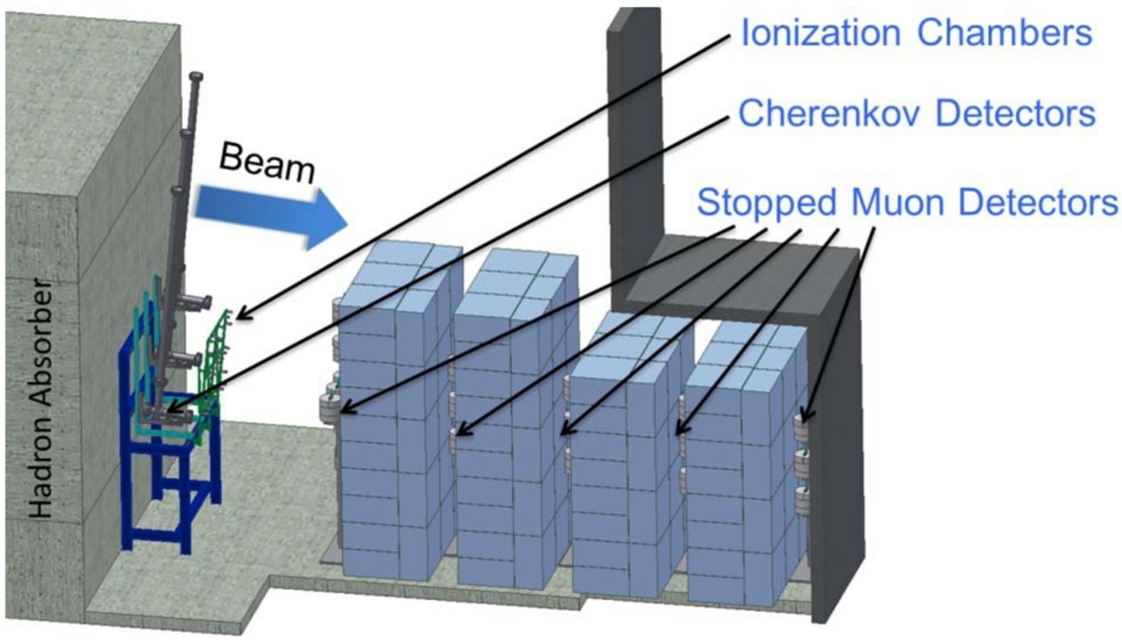

Figure 3.20: System of tertiary-beam muon detectors, located downstream of the LBNE beamline absorber, for monitoring the muon flux from the LBNE beamline.

In addition to the near neutrino detector, a sophisticated array of muon detectors will be placed just downstream of the absorber. The muon detectors, shown in Figure 3.20, detect mostly muons from the two-body decays of $\pi^{+(-)} \to \mu^{+(-)}\nu_\mu(\overline{\nu}_\mu)$ in the beamline, thus the measured muon and ν_μ flux distributions are highly correlated. The ionization chamber array will provide pulse-by-pulse monitoring of the beam profile and direction. The variable-threshold gas Cherenkov detectors will map the energy spectrum of the muons exiting the absorber on an on-going basis. The stopped muon detectors will sample the lowest-energy muons, which are known to correlate with the neutrino flux above 3 GeV — equivalent to about half the neutrino flux near the first oscillation maximum — and a decreasing fraction of it at lower energy. This system, together with the existing level of understanding of the similar NuMI beam and experience in previous neutrino oscillation experiments, will provide additional constraints on the understanding of the neutrino beam, and will thus support and complement the near neutrino detector measurements.

The reference design for the near neutrino detector is a fine-grained tracker [16], illustrated in Figure 3.21. It consists of a $3 \times 3 \times 7.04$ m^3 straw-tube tracking detector (STT) and electromagnetic

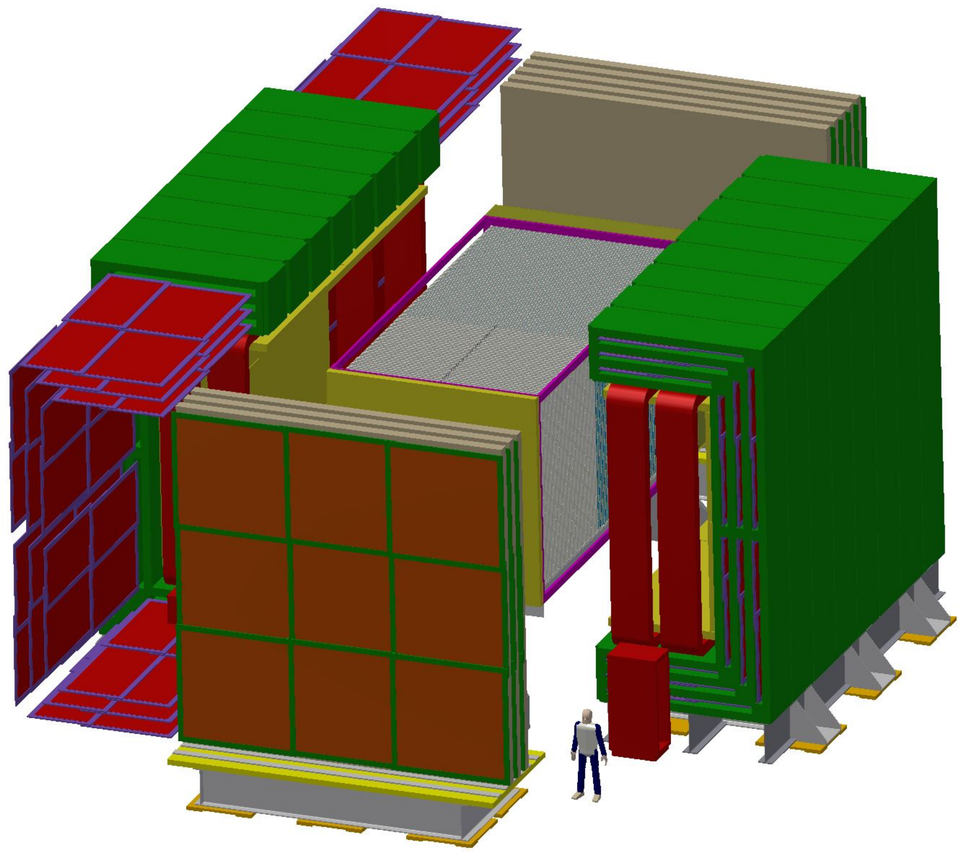

Figure 3.21: The LBNE near neutrino detector reference design with the dipole magnet open to show the straw-tube tracker (grey) and electromagnetic calorimeter (yellow). RPCs for muon identification (red squares) are embedded in the yoke steel and up- and downstream steel walls.

calorimeter inside of a 0.4-T dipole magnet, illustrated in Figure 3.22, and resistive plate chambers for muon identification (MuID) located in the steel of the magnet and also upstream and downstream of the tracker. High-pressure argon gas targets, as well as water and other nuclear targets, are embedded in the upstream part of the tracking volume. The nominal active volume of the STT corresponds to eight tons of mass. The STT is required to contain sufficient mass of argon gas in tubes (Al or composite material) to provide at least a factor of ten more statistics than expected in the far detector. Table 3.4 summarizes the performance for the fine-grained tracker's configuration, and Table 3.5 lists its parameters.

Figure 3.22 shows the locations of the electromagnetic calorimeter and MuID next to the magnet steel and magnet coils. The fine-grained tracker has excellent position and angular resolutions due to its low-density (~ 0.1 g/cm^3), high-precision STT. The low density and magnetic field allow it to distinguish e^+ from e^- on an event-by-event basis. The high resolution is important for determining the neutrino vertex and determining whether the neutrino interaction occurs in a water or argon target. Electrons are distinguished from hadrons using transition radiation.

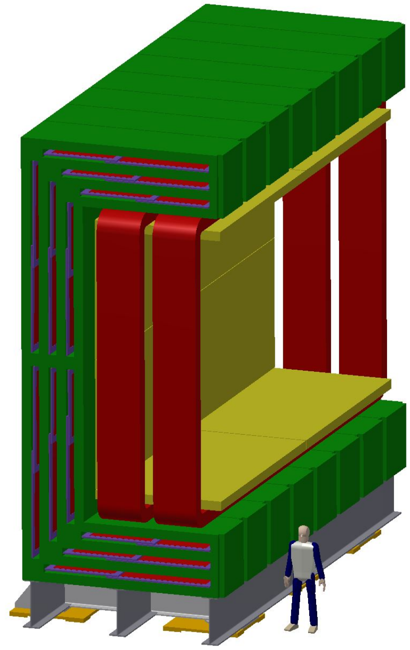

Figure 3.22: A schematic drawing of the ECAL (yellow modules) next to the magnet coils (red) and MuID (blue modules) interspersed in the magnet steel (green).

Table 3.4: Summary of the performance for the fine-grained tracker configuration

Performance Metric	Value
Vertex resolution	0.1 mm
Angular resolution	2 mrad
E_e **resolution**	5%
E_μ **resolution**	5%
$\nu_\mu/\overline{\nu}_\mu$ **ID**	Yes
$\nu_e/\overline{\nu}_e$ **ID**	Yes
NCπ^0**/CC**e **rejection**	0.1%
NCγ**/CC**e **rejection**	0.2%
NCμ**/CC**e **rejection**	0.01%

The design of the near neutrino detector is the subject of study by the LBNE Collaboration, and alternatives such as a magnetized liquid argon TPC will be investigated further. A detailed description of the fine-grained tracker can be found in [17], and descriptions of it and the alternative LArTPC design are presented in the March 2012 LBNE CDR (Volume 3 of [18]).

High-intensity neutrino beams can be used as probes of new physics and given the broad energy range of the LBNE beam, a diverse range of physics measurements is possible in the high-resolution near neutrino detector. These potentially wide-ranging physics measurements would complement other physics programs, such as those at Jefferson Laboratory, that are using proton,

Table 3.5: Parameters for the fine-grained tracker.

Parameter	Value
STT detector volume	$3 \times 3 \times 7.04$ m^3
STT detector mass	8 tons
Number of straws in STT	123,904
Inner magnetic volume	$4.5 \times 4.5 \times 8.0$ m^3
Targets	1.27-cm thick argon (~ 50 kg), water and others
Transition radiation radiators	2.5 cm thick
ECAL X_0	10 barrel, 10 backward, 18 forward
Number of scintillator bars in ECAL	32,320
Dipole magnet	2.4-MW power; 60-cm steel thickness
Magnetic field and uniformity	0.4 T; $< 2\%$ variation over inner volume
MuID configuration	32 RPC planes interspersed between 20-cm thick layers of steel

electron or ion beams from colliders and fixed-target facilities. A detailed discussion of the physics capabilities of a high-resolution near detector is presented in Chapter 7 and in [17].

3.6 Far Detector

The full-scope LBNE far detector is a liquid argon time-projection chamber of fiducial mass 34 kt located at the 4,850-ft level of the Sanford Underground Research Facility. The LArTPC technology allows for high-precision identification of neutrino flavors, offers excellent sensitivity to proton decay modes with kaons in the final state and provides unique sensitivity to electron neutrinos from a core-collapse supernova. The full detector size and its location at a depth of 4,850 feet will enable LBNE to meet the primary scientific goals — in particular, to find evidence for CP violation over a large range of $\delta_{\rm CP}$ values, and to significantly advance proton-decay lifetime limits. Conceptual designs of the 34-kt underground detector are well developed.

The liquid argon TPC technology chosen for LBNE combines fine-grained tracking with total absorption calorimetry to provide a detailed view of particle interactions, making it a powerful tool for neutrino physics and underground physics such as proton decay and supernova-neutrino observation. It provides millimeter-scale resolution in 3D for all charged particles. Particle types can be identified both by their dE/dx and by track patterns, e.g., the decays of stopping particles. The modest radiation length (14 cm) is sufficiently short to identify and contain electromagnetic showers from electrons and photons, but long enough to provide good e/γ separation by dE/dx (one versus two minimum ionizing particles) at the beginning of the shower. In addition, photons can be distinguished from electrons emanating from an event vertex by the flight path before their first interaction. These characteristics allow the LArTPC to identify and reconstruct signal events with high efficiency while rejecting backgrounds to provide a high-purity data sample. The principal design parameters of the full-scope LBNE LArTPC far detector are given in Table 3.6.

Table 3.6: Principal design parameters of the full-scope LBNE LArTPC far detector from [19].

Parameter	Value
Total/Active/Fiducial Mass	50/40/34 kt
Number of Detector Modules (Cryostats)	2
Drift Cell Configuration within Module	3 wide × 2 high × 18 long drift cells
Drift Cell Dimensions	2 × 3.7 m wide (drift) × 7 m high × 2.5 m long
Detector Module Dimensions	22.4 m wide × 14 m high × 45.6 m long
Anode Wire Spacing	∼5 mm
Wire Planes (Orientation from vertical)	Grid (0°), Induction 1 (45°), Induction 2 (-45°) Collection (0°)
Drift Electric Field	500 V/cm
Maximum Drift Time	2.3 ms

Scalability has been a design consideration of critical importance for the LBNE Project, and for the far detector in particular, since the Project's inception in 2009. A 10-kt LArTPC far detector configuration has been identified as the minimal initial configuration of LBNE that can make significant advances toward the primary scientific goals of LBNE. Because of the scalability built into the LBNE design, other, more capable, configurations could be accomplished either in the initial phase with the identification of additional resources, or at a later stage.

Other important considerations for the construction of LBNE's large LArTPC far detector include:

1. cryogenic safety and the elimination of hazards associated with large cryogenic liquid volumes

2. attainment of stringent argon purity requirements with respect to electronegative contaminants (e.g., < 0.2 ppb O_2 concentration)

3. ease of transport and assembly of TPC mechanical systems

4. efficient deployment of high-sensitivity/low-noise electronics for readout of the ionization signal

The far detector complex for both the first-phase ($\geq$ 10-kt) and full 34-kt options will be outfitted with two separately instrumented detector vessels instead of a single, larger vessel — an approach which has several benefits. First, this design enables each cryostat and TPC to be filled and commissioned while the other remains available for liquid storage, allowing for repairs to be made after the start of commissioning, should that be necessary. Secondly, it allows deployment of TPCs of different designs. This would enable, for example, international partners to contribute a detector of an alternate design, based on their own experience, or one that would emphasize a particular research interest.

The detector vessels will be constructed using technology standards from the liquefied natural gas (LNG) industry. With similar requirements and geometries, adaptation of industrial LNG cryostat design provides a high-performance, extensively tested approach to the challenge of liquid argon containment for LBNE. The cryostats in large LNG tanker ships are constructed using a thin (1–2 mm), polished, stainless steel inner membrane surrounded by thick foam passive insulation. With stainless steel as the only wetted surface, this is an inherently clean design, ideal for liquid argon detectors where high purity is essential.

The underground detector placement at the 4850L of the Sanford Underground Research Facility was studied in detail during the Conceptual Design Phase of LBNE and presented at the Fermilab Director's Independent Conceptual Design Review in March of 2012 [20]. Significant effort has been invested to minimize the (dominant) cost of the far site conventional facilities.

3.6.1 The 10-kt Detector Design

- The far detector for the initial phase of LBNE will have fiducial mass of *at least* 10 kt. This mass allows for high probability determination of the neutrino mass hierarchy and can provide evidence for CP violation, if this effect is large.
- The detector needs to be located deep underground to provide sensitivity for proton decay searches in the kaon modes and for measuring neutrinos from potential supernovae in the galaxy.
- A conceptual design for a 10-kt LArTPC has been developed, thoroughly reviewed and found to be sound.
- LBNE is working with international partners in an effort to deploy a more massive far detector in the initial phase.

A conceptual design for the initial 10-kt far detector for the first-phase LBNE Project has been developed that is easily scalable to larger detectors. Many of the detector elements, in particular the modular TPC design and readout electronics, utilize full-scale modules and designs that can easily be replicated in larger numbers to instrument a larger detector. This design consists of two

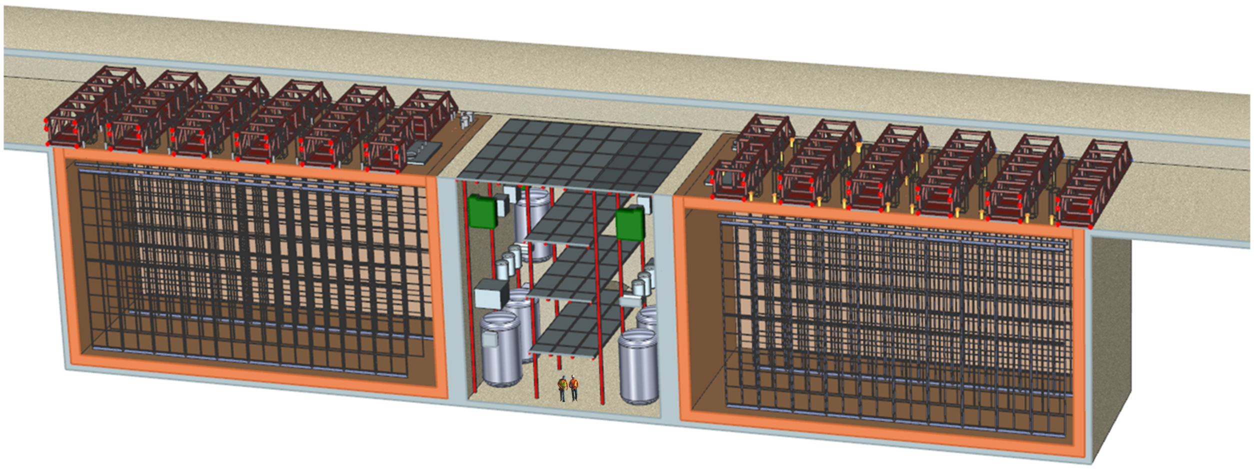

Figure 3.23: 3D view of the 10-kt far detector showing a lateral cross section of the two 5-kt fiducial-mass LArTPC vessels

9.4-kt liquid argon vessels [19], each designed to hold a 5-kt fiducial-mass LArTPC as shown in Figure 3.23.

The cryogenics systems for the 10-kt detector will consist of two 85-kW liquid nitrogen liquefaction plants, a liquid argon receiving station, a liquid argon circulation system with liquid purifiers, and a liquid argon re-condensing system. All the cryogenics systems are similar to large-scale systems found in industrial applications.

The LBNE TPC design for the 10-kt detector consists of three rows of cathode plane assemblies (CPAs) interspersed with two rows of anode plane assemblies (APAs), similar to the layout concept shown in Figure 3.24 bottom right, with readout electronics mounted directly on the APA frames (Figure 3.24, left). These elements run the length of a cryostat module, save for space at one end allocated to the cryogenics systems. A field cage for shaping the electric field covers the top, bottom, and ends of the detector. The spacing between the CPA and APA rows is 3.48 m and the cathode planes will be operated at 173 kV, establishing a drift field of 500 V/cm and a corresponding maximum drift time of 2.16 ms.

The APAs and CPAs are designed in a modular fashion as illustrated in Figure 3.24, top right. Each APA/CPA is constructed with a support frame 2.5 m long and 7 m high; these dimensions are chosen for ease of transportation to the detector site and installation within the cryostat. During installation, two APAs are connected end-to-end to form a 14 m tall, 2.5 m long unit, which is transported to its final position in the detector and suspended there using a rail system at the top of the detector. Pairs of CPAs are installed in a similar fashion. This system of 2.5 m long detector elements is easily scalable to any desired detector size. A total of 40 APAs and 60 CPAs per cryostat are needed for the 10-kt detector design, configured as two rows of APAs, ten APA pairs long.

Three sense wire planes (two *induction* planes and one *collection* plane) with wire pitches of 4.8

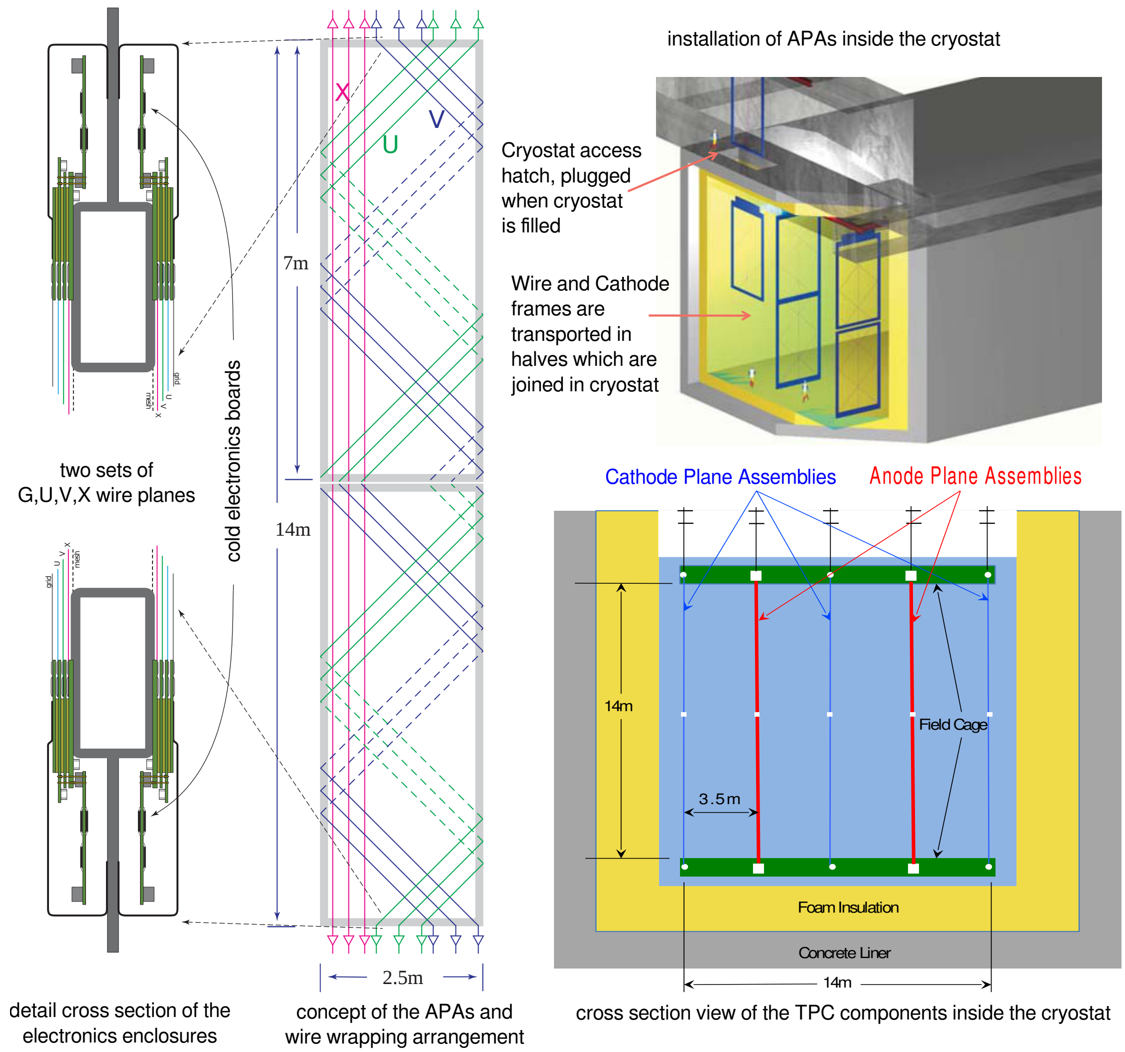

Figure 3.24: The LBNE TPC modular construction concept

mm are mounted on each side of an APA frame, for sensitivity to ionization signals originating within the TPC cell on either side. The wires on these planes are oriented vertically (collection) and at $\pm 45°$ (induction)¶. The induction plane wires are wrapped around the APA frame, and are therefore sensitive to charge arriving from either side of the APA, depending on where the charge arrives along the length of the wires. This configuration allows placement of readout electronics at the top and bottom of each two-APA unit. (Cables from the bottom APA are routed up through the support frame, thereby eliminating any obstruction they would otherwise cause.) In this way, adjacent APA-pairs can be abutted so as to minimize the uninstrumented region in the gaps between them along the length of the detector.

¶The current design uses a 36° orientation to remove hit assignment ambiguities.

Low-noise, low-power CMOS (Complementary Metal Oxide Semiconductor) preamplifier and ADC ASICS (Application Specific Integrated Circuit) have been developed for deployment on circuit boards mounted directly on the APA frames. This scheme ensures good signal-to-noise performance, even allowing for some attenuation of long-drift ionization signals due to residual impurities in the argon. It also offers the possibility of digital signal processing, including multiplexing and zero suppression at the front end, thereby limiting the cable plant within the cryostat and the number of penetrations required, while also easing requirements on the downstream read-out/DAQ systems located outside the cryostat. The ASICS have been laid out following design rules developed explicitly for long-term operation at cryogenic temperatures.

In order to separate neutrino beam events from other interactions — particularly for proton decay and supernova neutrino signals — it is necessary to accurately determine the event time relative to the neutrino beam time window or an incoming cosmic muon. If the event time is known at the microsecond level then out-of-time cosmic-ray backgrounds for beam neutrinos can be rejected to the level of 10^{-5} (the beam spill duty factor). The slow ionization-electron drift velocity gives the TPC its 3D imaging capability, but an independent fast signal is required to localize events in time and in space along the drift direction. The excellent scintillation properties of liquid argon ($\mathcal{O}(10^4)$ photons per MeV of energy deposition) are exploited to address this issue. A photon detection system is planned for detection of the 128-nm scintillation light that, in turn, allows determination of the event timing. Several photon detector designs are under study. The most advanced design uses cast acrylic bars coated with wavelength shifter, and SiPMs (silicon photomultipliers) at the ends for read-out. These bars will be assembled into paddles of dimensions 10 cm by 2 m, and mounted on the APA frames, fitting within the 5-cm gap between the sets of wire planes located on both sides of the frames. Initial studies indicate a light yield of 0.1 to 0.5 photoelectrons per MeV.

3.6.2 The 34-kt Detector Design

One possible design of a 34-kt detector is two 17-kt modules placed end-to-end in a common cavern at the 4,850-ft level of the Sanford Underground Research Facility, as shown in Figure 3.25. This design was reviewed at the Fermilab Director's Independent Conceptual Design Review in March of 2012 [20].

Alternatively, the 34-kt detector can be realized by adding a roughly 24-kt detector of essentially the same design as the 10-kt detector, housed in a set of two cryostats, each holding 12 kt (20 kt total) of liquid argon. In this configuration the additional cryostats each have three APA rows (total 84 APAs) and four CPA rows (total 112 CPAs), making them wider than the 10-kt design described in Section 3.6.1. The APA-to-CPA row spacing is expanded to 3.77 m and the length of each is increased to 14 APA units long.The cryogenics system installed for the 10-kt design will simply be expanded from two to four 85-kW refrigerators to service both the 10-kt and the 24-kt detector. The 24-kt detector hall will be excavated parallel to the 10-kt detector hall as shown in Figure 3.26.

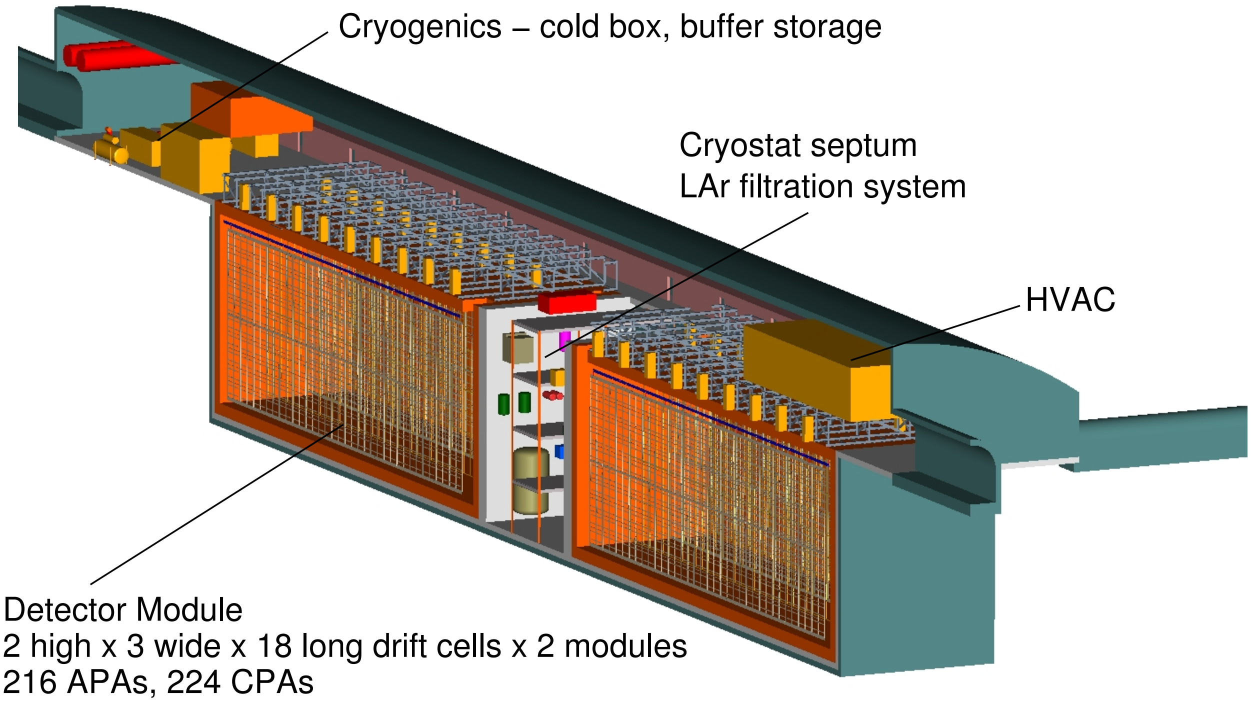

Figure 3.25: Schematic of a 34-kt LArTPC design. The detector comprises two 17-kt LArTPC vessels.

Given the modular design of the detector and the use of industrial technologies in the cryogenics system, there is a great deal of flexibility in possible contributions from new partners to expand the size of the detector. The details of any scope change would depend on the interests, capabilities and resources of the new partners.

A full geotechnical site investigation is underway to characterize the rock mass in which it is planned to site the LBNE far detector. Mapping of existing drifts in the vicinity of the proposed detector location has been completed and a core boring program was launched in early 2014. This investigation will explore the area with enough breadth to allow flexibility in siting and sizing detector modules in the future before design work begins. The proposed boring layouts are shown in Figure 3.27 overlaid with possible 34-kt and 70-kt modules to demonstrate the large capacity of this location.

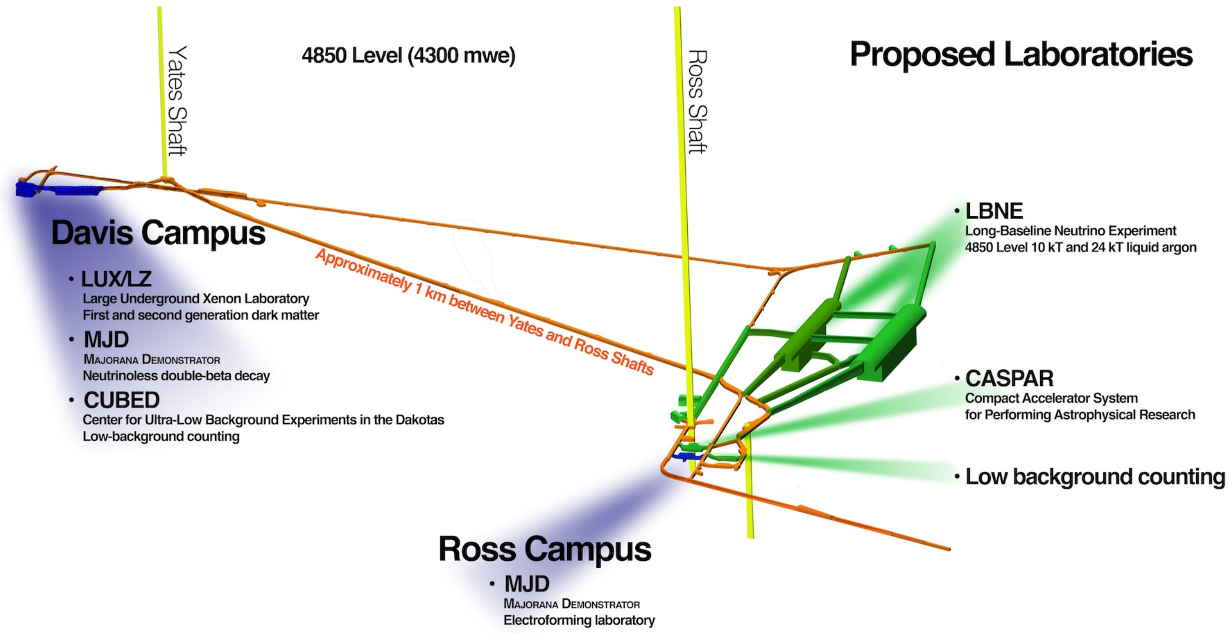

Figure 3.26: Layout of the 10-kt + 24-kt LArTPC detector halls at the 4,850-ft level of the Sanford Underground Research Facility.

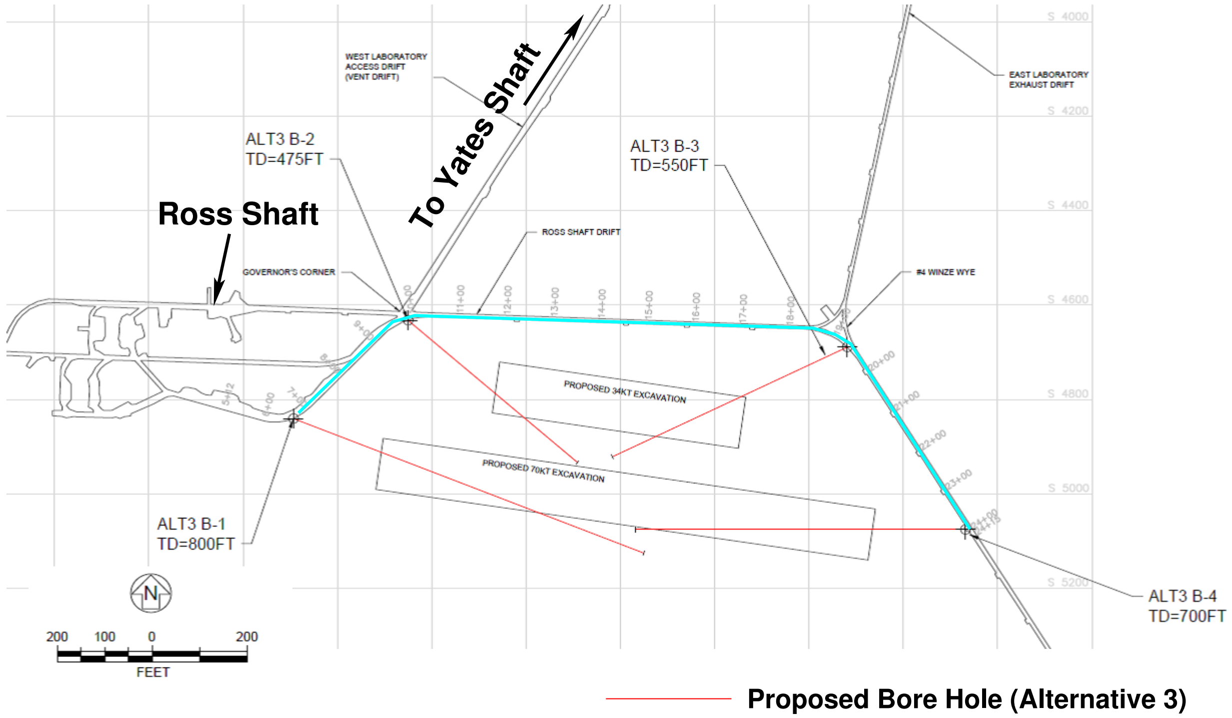

Figure 3.27: Geotechnical site investigation plan, showing the drifts that have been mapped (blue) and the planned core borings (red) overlaid on possible locations of caverns that would accommodate the 34-kt or larger (70-kt shown as an example) LArTPC detectors.

References

1. Particle Physics Project Prioritization Panel, "U.S. Particle Physics: Scientific opportunities, a plan for the next ten years.". May, 2008. `http://science.energy.gov/~/media/hep/pdf/files/pdfs/p5_report_06022008.pdf`. Cited in Sections 3.1 (pg.46) and 3.2 (pg.48).
2. DOE Office of Science, Office of High Energy Physics, "Mission Need Statement for a Long-Baseline Neutrino Experiment (LBNE)," DOE, `LBNE-doc-6259`, 2009. Cited in Section 3.1 (pg.47).
3. M. Bass *et al.*, **LBNE Collaboration** , "Baseline optimization for the measurement of CP violation and mass hierarchy in a long-baseline neutrino oscillation experiment," FERMILAB-PUB-13-506-E, `arXiv:1311.0212 [hep-ex]`, 2013. Cited in Section 3.1 (pg.47).
4. Derwent, P. and others, "Proton Improvement Plan II," Project X-doc-1232, November, 2013. Cited in Sections 3.2 (pg.51) and 3.4 (pg.63).
5. S. Holmes, R. Alber, B. Chase, K. Gollwitzer, D. Johnson, *et al.*, "Project X: Accelerator Reference Design," FERMILAB-TM-2557, BNL-101116-2013-BC-81834, JLAB-ACP-13-1725, PNNL-22523, SLAC-R-1020, UASLP-IF-13-001, `arXiv:1306.5022 [physics.acc-ph]`, 2013. Cited in Section 3.2 (pg.51).
6. "Sanford Underground Research Facility." `http://www.sanfordlab.org`. Cited in Section 3.3 (pg.54).
7. B. Cleveland, T. Daily, R. Davis Jr., J. R. Distel, K. Lande, *et al.*, "Measurement of the solar electron neutrino flux with the Homestake chlorine detector," *Astrophys.J.* **496** (1998) 505–526. Cited in Section 3.3 (pg.54).
8. F. Gray, C. Ruybal, J. Totushek, D.-M. Mei, K. Thomas, *et al.*, "Cosmic Ray Muon Flux at the Sanford Underground Laboratory at Homestake," *Nucl.Instrum.Meth.* **A638** (2011) 63–66, `arXiv:1007.1921 [nucl-ex]`. Cited in Section 3.3 (pg.58).
9. W. Roggenthen and A. Smith, "U, Th, K contents of materials associated with the Homestake DUSEL site, Lead, South Dakota," *Private Communication* . Cited in Section 3.3 (pg.59).
10. D. Akerib *et al.*, **LUX Collaboration** , "First results from the LUX dark matter experiment at the Sanford Underground Research Facility," `arXiv:1310.8214 [astro-ph.CO]`, 2013. Cited in Section 3.3 (pg.59).
11. **LBNE Project Management Team** , "LBNE Conceptual Design Report, Volume 2: The Beamline at the Near Site," `LBNE-doc-4317`, 2012. Cited in Section 3.4 (pg.63).
12. M. Bishai and Y. Lu, "Conceptual Designs for a Wide-Band Low-Energy Neutrino Beam Target," `LBNE-doc-3151`, November, 2010.
13. B. Lundberg, "A beginner guide to horn design and history of LBNE horn design," `LBNE-doc-8398`, November, 2014.

14. D. Ayres *et al.*, **NOvA Collaboration** , "The NOvA Technical Design Report," FERMILAB-DESIGN-2007-01, 2007. `http://lss.fnal.gov/archive/design/fermilab-design-2007-01.pdf`. Cited in Section 3.4 (pg.63).
15. E. Worcester, "Potential Sensitivity Improvements with 10 kT LBNE," `LBNE-doc-6599`, 2012. Cited in Section 3.4 (pg.69).
16. S. Mishra, R. Petti, and C. Rosenfeld, "A High Resolution Neutrino Experiment in a Magnetic Field for Project-X at Fermilab," *PoS* **NUFACT08** (2008) 069, `arXiv:0812.4527 [hep-ex]`. Cited in Section 3.5 (pg.71).
17. B. Choudhary *et al.*, **Indian Institutions and Fermilab Collaboration** , "LBNE-India Detailed Project Report (DPR) submitted to DAE, India," `LBNE-doc-6704`, 2012. Cited in Sections 3.5 (pg.73) and 3.5 (pg.74).
18. **LBNE Project Management Team** , "LBNE Conceptual Design Report, Volume 3: Detectors at the Near Site," `LBNE-doc-4724`, 2012. Cited in Section 3.5 (pg.73).
19. **LBNE Project Management Team** , "LBNE Conceptual Design Report, Volume 4: The Liquid Argon Detector at the Far Site," `LBNE-doc-4892`, 2012. Cited in Section 3.6.1 (pg.77).
20. "Final Report, Director's Independent Conceptual Design and CD-1 Readiness Review of the LBNE Project," `LBNE-doc-5788`, March, 2012. Cited in Sections 3.6 (pg.76) and 3.6.2 (pg.79).